Lens-Type Redirective Reconfigurable Intelligent Surfaces for Multi-User MIMO Communications

by

Md Jawwad Chowdhury

A Thesis submitted to The Faculty of Graduate Studies of

The University of Manitoba

in partial fulfillment of the requirements for the degree of

Master of Science

Department of Electrical and Computer Engineering

University of Manitoba

Winnipeg

December 2022

Abstract

Reconfigurable intelligent surfaces (RIS), also known as smart repeaters, have been widely adopted in the open literature as a low-cost, energy-efficient solution to tackle the blockage problem in existing wireless networks. In this thesis, we first introduce the idea of using *redirective* reconfigurable intelligent surfaces (RedRIS) to overcome many of the challenges associated with the conventional *reflective* RIS. We develop a framework for jointly optimizing the switching matrix of the lens-type RedRIS ports along with the active precoding matrix at the base station (BS) and the receive scaling factor. A joint non-convex optimization problem is formulated under the minimum mean-square error (MMSE) criterion with the aim to maximize the spectral efficiency of each user. In the single-cell scenario, the optimum active precoding matrix at the multi-antenna BS and the receive scaling factor are found in closed-form by applying Lagrange optimization, while the optimal switching matrix at the lens-type RedRIS is obtained by means of a newly developed alternating optimization algorithm. We then extend the framework to the multi-cell scenario with single-antenna base stations that are aided by the same lens-type RedRIS. We further present two methods for reducing the number of effective connections of the RedRIS ports that result in appreciable overhead savings while enhancing the robustness of the system.

The proposed RedRIS-based schemes are gauged against reflective RIS-based systems under both perfect and imperfect channel state information (CSI). The simulation results show the superiority of the proposed schemes in terms of overall throughput with much less control overhead.

Dedicated to my beloved son, *"Aariz"*, who came as a source of happiness during this research.

Acknowledgements

Table of Contents

List of Figures

List of Tables

List of Abbreviations

B5G	Beyond 5G
BS	Base station
CSI	Channel state information
LMMSE	Linear minimum mean square error
LOS	Line-of-sight
MIMO	Multiple-input multiple-output
MISO	Multiple-input single-output
MMSE	Minimum mean square error
MSE	Mean square error
NLOS	Non-line of sight
RedRIS	Redirective reconfigurable intelligent surface
RIS	Reconfigurable intelligent surface
SINR	Signal to interference plus noise ratio
SVD	Singular value decomposition
VAMP	Vector approximate message passing

Chapter 1

Introduction

1.1 Overview

Wireless communication technology is developing at a fast pace to meet the ever-growing demands for higher data rates and massive connectivity. The soaring number of users in the network is exacerbating the interference problem which limits the performance of legacy wireless networks. To resolve the problem of spectrum shortage, the wireless technology is migrating to higher frequency bands to leverage the under-utilized spectra [1]. With the fifth-generation (5G) mmWave communication technology being currently available to a limited demography, researchers have already started exploring the feasibility of using the Terahertz (THz) band in beyond 5G (B5G) networks [2,3]. However, THz communication faces many challenges such as severe wireless propagation loss and difficulties related to transceiver design [4,5]. Recently, the reconfigurable intelligent surface (RIS) technology has emerged as a cost-effective solution for purposely controlling the radio propagation environment to extend the wireless coverage and better mitigate the interference issues [6–9]. The widely studied reflective RIS consists of a planar metasurface with several passive reflective elements which alter the incident

signal by means of adaptively configured phase shifters. The main advantages of RISs are enlisted as follows [10]:

- **Easy deployment:** Reflective RISs are mostly passive devices made of electromagnetic (EM) metasurfaces. RISs can be easily deployed on several existing structures such as building facades, indoor walls, aerial platforms, roadside billboards, highway polls, vehicle windows, as well as pedestrians' clothes due to their low-cost.

- **Environment friendly:** Unlike the traditional relaying systems or repeaters, RISs don't need power amplifier to reshape the incoming signal. Instead, reflective RISs can reshape the wireless signal by reconfiguring the phase shifts of its reflective elements which make it an environment friendly system.

- **Improvement of spectral efficiency:** Power loss over long-distance communication can be overcome with the use of RIS as they are able to control the wireless propagation environment. In fact, RIS can be used for passive beamforming purposes. Passive beamforming refers to perform beamforming without having any requirement for actively powering the elements. This improves the received power while reducing the inter-user-interference resulting in increase in the user throughput [8]. In typical urban areas, where there is no line of sight (LOS) between the BSs and the users, RISs can be deployed to assist the communication and thereby enhance the overall spectral efficiency.

- **Integration with the existing networks:** RIS can be seamlessly integrated with the existing 4G, 5G and B5G networks without any technical difficulties. RIS also support full-duplex transmission mode.

Fig. 1.1 illustrates some of the diversified applications of RIS in wireless communication networks. The main applications of RIS are in the fields of but not limited to the

6G wireless networks, RIS-aided autonomous vehicle communications, RIS-aided drone communications, RIS-aided IoT communications and RIS-aided mobile edge computing [11].
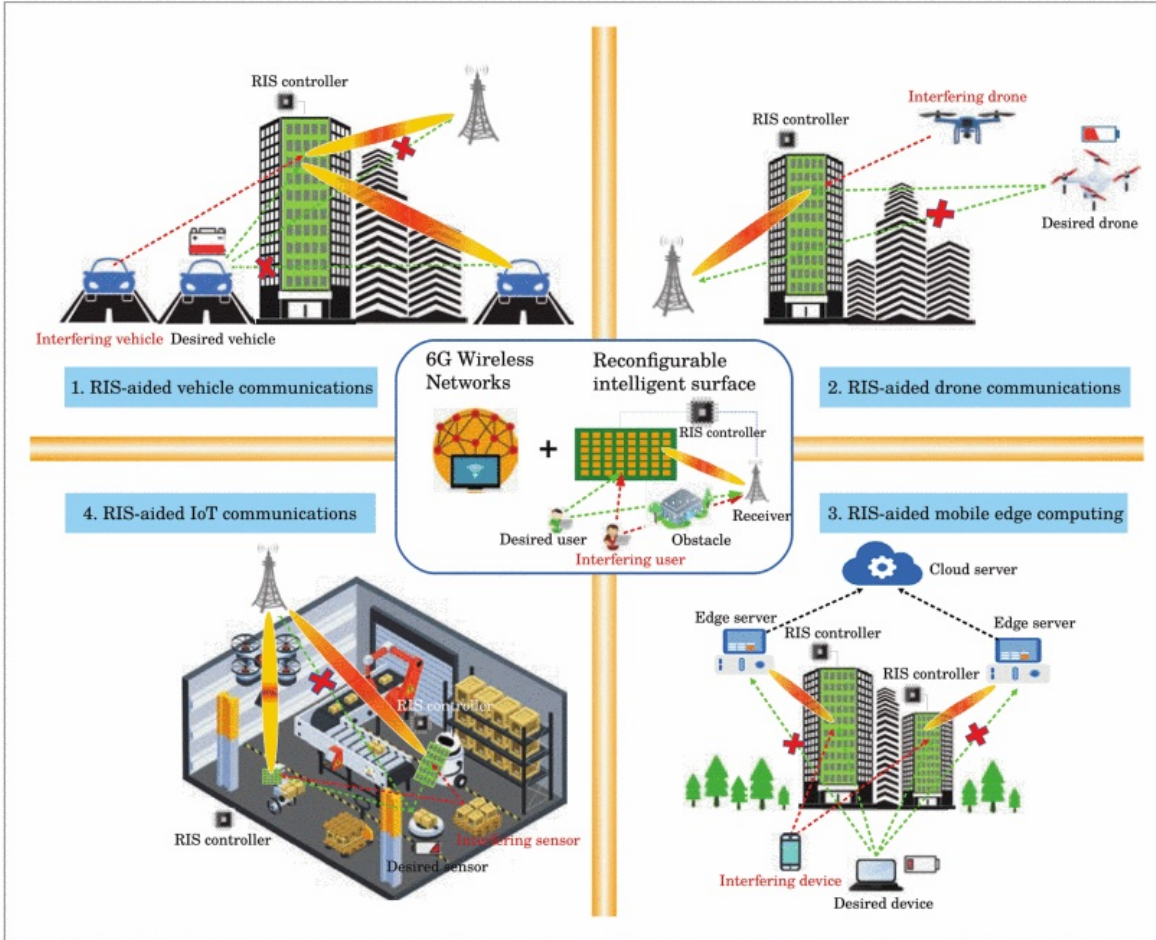
Figure 1.1: Applications of conventional RIS [11].

- **RIS-aided B5G/6G wireless networks:** Fig. 1.1 illustrates an RIS-aided cellular system designed for energy-efficient green 6G services that typically supports a number of mobile devices. It has also numerous applications in the enhanced device to device (D2D) networks. Moreover, RIS can be utilized for energy harvest-

ing purpose in the simultaneous wireless power and information transfer (SWIPT) networks [12].

- **RIS-assisted vehicle communications:** The concept of autonomous vehicle is being much discussed in recent days. To ensure instantaneous communication with the self-driven vehicles through cellular network, RIS can be used as a low-cost intelligent solution to provide higher data-rates.

- **RIS-aided drone communications:** In recent days, AI-based unmanned aerial vehicles, also known as drones have been widely adopted in various civil, commercial and military services. RIS can be used as a low-cost, passive device to communicate with the drones from base stations without consuming the drone propulsion energy.

- **RIS-aided Internet of Things (IoT) communications:** IoT is a recent concept of connecting all the devices through internet and remotely control them. Majority of the domestic devices remain inside the buildings which impede their connectivity to the remote base stations. To overcome the blockage problem, RIS can become an outstanding solution to enhance the connectivity and make IoT a success.

- **RIS-aided mobile edge computing:** The mobile edge computing concept includes an edge server located at a remote place that communicates with the end users by means of low-latency communication channel. Interference signals from the unexpected users pose a problem to this new concept of communication. RIS can be easily installed at suitable places to reroute the signal from the edge server to the desired users to overcome the interference.

Due to the many advantages and diversified applications, reflective RIS has significantly drawn the attention of the researchers in recent years. However, the control overhead

and complexity of the reflective RIS increase substantially with the number of reflective elements [13].

1.1.1   Challenges in Reflective RIS-Aided Communications

We discuss couple of challenges encountered in reflective RIS-aided wireless networks:

- **Necessity of accurate CSI (channel state information):** Despite the necessity of accurate CSI knowledge in MIMO and MISO RIS wireless communication networks, it is challenging to acquire the information at prior because this needs considerable training overhead. In addition, the residual error in the CSI may lead to error in RIS configuration which will result in unexpected behavior in the RIS-aided communication.

- **Optimization of phase shifting elements:** Conventional reflective RIS contains numerous phase shifts used as reflective elements. The use of phase shifts is challenging in the aspect of control overhead and related hardware impairments. Also, the controlling circuit is complex in nature. To achieve the best result from the RIS system, it is imperative to overcome the challenges related to the phase-shifts-based reflective RIS.

To overcome many of the challenges associated with the widely-studied reflective RIS, we introduce the idea of using a lens-type redirective RIS (called RedRIS) which inherently relies on designing the beamforming vectors that redirect the incident wireless signals to the intended users. The main advantages of the redirective RIS over the reflective RIS are listed as follows:

- **Beamspace switching:** In the lens-type RedRIS, beamspace switching and DFT codebook is used unlike the phase shifting elements in the reflective RIS. The

use of beamspace switching makes the RedRIS system simpler and lessens the operational complexity.

- **Less control overhead:** Control of the RedRIS is easier compared to the phase shifting elements based reflective RIS as only back-to-back connection is required for the switching of its ports. In fact, the control overhead scales only logarithmically with the redirective RIS size as opposed to the reflective RIS where the control overhead scales linearly with the number of antennas [14, 15].

- **Integration of power amplifiers:** Although the lens-type RedRIS is a passive network element, it can be integrated with two-port amplifiers as opposed to the reflective RIS which would require reflection-mode amplifiers where achieving the stability becomes a major challenge [14, 16].

- **Simplified control device:** The controlling device of the RedRIS is much simpler and easy to use as it only acts like an on/off switch to control the back-to-back connections among the RedRIS ports.

In addition, all the other advantages of conventional reflective RIS are also applicable to the lens-type RedRIS.

1.2   Related Work and Contributions

Significant research effort has been made towards the design of the reflective RIS for passive beamforming purposes in single-user MIMO communications [17–26]. Recently, a VAMP-based algorithm has also been developed to optimize the phase shifts of the reflective RIS in the multi-user MIMO setting [27]. However, the concept of using the lens-type redirective surfaces as RIS is novel and to our best of knowledge, the use of

lens-type RedRIS for electromagnetic radiation control has not been investigated in the open literature.

1.3 Motivation

In this thesis, we introduce the idea of using a lens-type redirective RIS (called RedRIS) whose back-to-back port connections can be appropriately configured to select the beamforming vectors which redirect the incident signals towards their intended users. Such beamforming vectors are selected from a DFT codebook that scans all the directions of radiation [28], without the need of any phase shifting element. In Chapter 3, we propose a general framework which involves the optimization of the back-to-back connections (or switching matrix) between the RedRIS ports, as opposed to finding the optimal phase shifts in the purely reflective RIS. Interestingly, the proposed switching mechanism drastically reduces the incurred signaling overhead and operational complexity for RIS-aided systems. We extend the framework to multi-cell scenario with single-antenna base stations, assisted by the same RedRIS in Chapter 4. To the best of our knowledge, the use of lens-type RedRIS for electromagnetic radiation control has not been investigated in the existing literature. We name such lens-type smart surface as redirective RIS (RedRIS) due to its capabilities of wirelessly redirecting the impinging waves to their intended destinations in the downlink and uplink modes alike. We use the names RedRIS and lens-type RIS interchangeably throughout the thesis.

1.4 Thesis Organization and Notations

The rest of the thesis is organized as per the following sequence::

- In Chapter 2, the beamforming design of conventional reflective RIS is discussed by reviewing the work on jointly optimizing the reflection coefficients of the reflective

RIS along with the BS precoding matrix and the receive scaling factor [29].

- In Chapter 3, we introduce the idea of lens-type RedRIS, and propose a framework of jointly optimizing the precoding matrix at the BS and the ports switching matrix of the RedRIS. Moreover, we develop a new algorithm for the joint optimization. Also, we discuss two methods for reducing the number of RedRIS port connections for the single- and multi-user cases.

- Extension of the proposed framework to the multi-cell scenario is provided in Chapter 4.

- Chapter 5 mentions some future research directions before drawing the conclusion.

Notations: In this paper, scalar variables are represented by lower-case italic letters (e.g., x). Lower- and upper-case bold fonts, $\mathbf{x}$ and $\mathbf{X}$, are used to denote vectors and matrices, respectively. The (m,n)th entry of $\mathbf{X}$ is denoted as $\mathbf{X}_{mn}$, and the nth element of $\mathbf{x}$ is denoted as x_n. Rank$(\mathbf{X})$ and Tr$(\mathbf{X})$, return the rank and the trace of $\mathbf{X}$, respectively. The identity, all-ones, and all-zero matrices of size $N \times N$ are denoted as $\mathbf{I}_N$, $\mathbf{J}_N$, and $\mathbf{0}_N$, respectively. Moreover, diag(.) operates on a matrix to return its main diagonal elements in a vector, whereas Diag$(\mathbf{X})$ sets the off-diagonal elements of $\mathbf{X}$ to zero and Diag$(\mathbf{x})$ returns a diagonal matrix whose main diagonal is $\mathbf{x}$. The shorthand notation $\mathbf{x} \sim \mathcal{CN}(\mathbf{x}; \mathbf{m}, \mathbf{R})$ means that the random vector $\mathbf{x}$ follows a complex circular Gaussian distribution with mean $\mathbf{m}$ and covariance matrix $\mathbf{R}$. Moreover, $(.)^*$, $(.)^\mathsf{T}$, and $(.)^\mathsf{H}$ stand for the conjugate, transpose, and Hermitian (transpose conjugate) operators, respectively. We use vec(.) and unvec(.) to denote vectorization of a matrix and unvectorization of a vector back to its original matrix form, respectively. In addition, $|.|$, $\|.\|_2$ and $\|.\|_\mathrm{F}$ stand for the modulus, Euclidean norm, and Frobenius norm, respectively. The cardinal of a set $\mathcal{E}$ is denoted as $|\mathcal{E}|$ and $\Re\{.\}$ stands for the real part of

its complex-valued argument. The statistical expectation is denoted as $\mathbb{E}\{.\}$, and the operator $\otimes$ denotes the Kronecker product between two matrices.

Chapter 2

Reflective RIS for Wireless Communications

Reconfigurable intelligent surface (RIS), also called Intelligent reflective surface (IRS) is a recently introduced, promising technology to improve the spectral efficiency of wireless networks by purposely controlling the propagation environment of electromagnetic waves [30,31]. The conventional reflective RIS is formed of a passive planar metasurface constituting of many reflective elements. A controller is attached to the RIS to dynamically reconfigure the phase shifts of the reflective RIS elements [32]. In this chapter, we briefly review the beamforming design and performance of a reflective RIS-aided MU-MIMO communication system in the downlink single-cell setup [29]. The reflective RIS consists of a number of phase shifting elements that assists the BS to reroute the signal to its intended users. A framework is described to optimize the joint beamforming of the BS precoding matrix along with the phase shifts of the reflective elements of the RIS. The following topics are mainly reviewed in this chapter:

- A problem is formulated to jointly optimize the reflection coefficients of the reflective RIS along with the BS precoding matrix and the receive scaling factor.

- The formulated joint optimization problem is separated into two smaller sub-optimization problems by applying alternating minimization technique [33].

- The BS precoding matrix and the receive scaling factor is optimized in a closed-form solution by following Lagrange optimization [27].

- The reflection coefficients of the reflective RIS are efficiently optimized using a modified version of the VAMP algorithm [34].

- Numerical results are presented to compare the performance of the reflective RIS with the state-of-the-art solutions.

The rest of the chapter is organized as follows: the system model along with the problem formulation are discussed in Section 2.1. Section 2.2 briefly describes the modified VAMP algorithm and solving the joint optimization problem using it. Finally, sample numerical results are shown in Section 2.3.

2.1 System Model, Assumptions, and Problem Formulation

Consider a BS having N antenna elements and serving M ($M < N$) single-antenna users in the downlink. A reflective RIS, having K ($K > M$) reflective elements is placed in between to assist the communication. The vector $\mathbf{h}_{\text{b-u},m} \in \mathbb{C}^N$ denotes the m-th link between the BS-user channel. Similarly, for the reflevtive RIS-user channel, the m-th link is expressed with $\mathbf{h}_{\text{s-u},m} \in \mathbb{C}^K$. The channel matrix for the link between the reflective RIS and the BS is denoted by $\mathbf{H}_{\text{b-s}} \in \mathbb{C}^{K \times N}$. Figure 2.1 illustrates the high-level view of the reflective RIS-assisted communication. The incident signal from the BS is phase-shifted by the reflective elements of the RIS which is expressed by means of
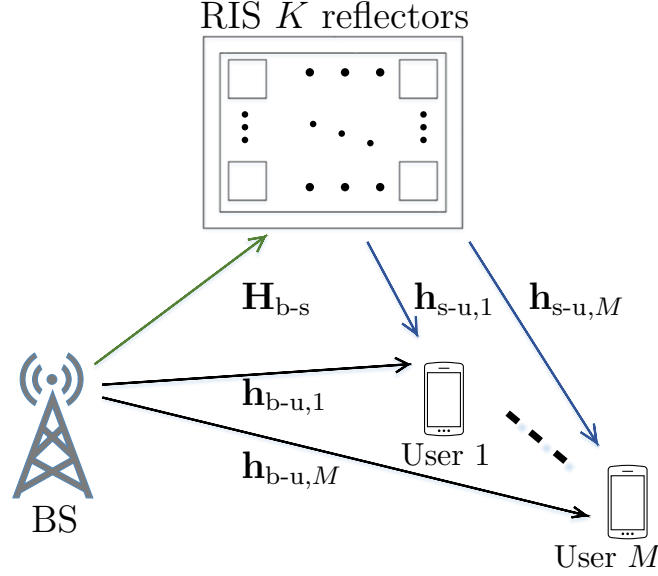
Figure 2.1: Reflective RIS-assisted wireless communication [29].

a diagonal matrix $\text{Diag}(\boldsymbol{v}) \in \mathbb{C}^{K \times K}$, where $\boldsymbol{v} \in \mathbb{C}^K$ is the phase-shifting vector having unimodular elements, i.e., $|v_k| = 1$ for $k = 1, \dots, K$.

The signal received by the user-m can be expressed in terms of the channel links as:

$$\mathsf{y}_m = \mathbf{h}_{\text{s-u},m}^{\mathsf{H}} \text{Diag}(\boldsymbol{v}) \mathbf{H}_{\text{b-s}} \sum_{m'=1}^{M} \mathbf{f}_{m'} \mathsf{s}_{m'} + \mathbf{h}_{\text{b-u},m}^{\mathsf{H}} \sum_{m'=1}^{M} \mathbf{f}_{m'} \mathsf{s}_{m'} + \mathsf{w}, \quad m = 1, \dots, M \quad (2.1)$$

where $\mathsf{s}_m \sim \mathcal{CN}(s; 0, 1)$ is the unknown symbol transmitted by user-m and $\mathsf{w} \sim \mathcal{CN}(w; 0, \sigma_{\text{w}}^2)$ denotes additive white Gaussian noise (AWGN). Here, $\mathbf{f}_m \in \mathbb{C}^N$ for $m = 1, \cdots, M$ represent the BS precoding vectors used for the power allocation during beamforming. By stacking all the entities in respective vectors/matrices, we express the received signal of all users in terms of the channel links and precoding matrix as:

$$\mathbf{y} = \underbrace{\mathbf{H}_{\text{s-u}}^{\mathsf{H}} \text{Diag}(\boldsymbol{v}) \mathbf{H}_{\text{b-s}} \mathbf{F} \mathbf{s}}_{\text{Users-RIS-BS}} + \underbrace{\mathbf{H}_{\text{b-u}}^{\mathsf{H}} \mathbf{F} \mathbf{s}}_{\text{Users-BS}} + \mathbf{w}. \quad (2.2)$$

The optimization problem is formulated under the sum MMSE criterion to minimize

the received symbol error of each user as follows:

$$\underset{\alpha,\mathbf{F},\boldsymbol{v}}{\arg\min} \quad \mathbb{E}_{\mathbf{y},\mathbf{s}}\left\{\|\alpha\mathbf{y}-\mathbf{s}\|_2^2\right\}, \tag{2.3a}$$

$$\text{subject to} \quad \mathbb{E}_{\mathbf{s}}\left\{\|\mathbf{Fs}\|_2^2\right\}=P, \tag{2.3b}$$

$$|v_i|=1, \quad i=1,2,\cdots,K. \tag{2.3c}$$

Here, $\alpha \in \mathbb{R}$ denotes the receive scaling factor [35,36]. By recalling the expectation of $\mathbf{y}$ in 2.2 and resorting to some algebraic manipulations, it can be shown that the objective function in (2.3a) is equivalent to:

$$\underset{\alpha,\mathbf{F},\boldsymbol{v}}{\arg\min} \quad \left\|\alpha\mathbf{H}_{\text{s-u}}^{\mathsf{H}}\text{Diag}(\boldsymbol{v})\mathbf{H}_{\text{b-s}}\mathbf{F}-(\mathbf{I}_M-\alpha\mathbf{H}_{\text{b-u}}^{\mathsf{H}}\mathbf{F})\right\|_{\text{F}}^2+M\alpha^2\sigma_{\text{w}}^2, \tag{2.4a}$$

$$\text{s.t.} \quad \|\mathbf{F}\|_{\text{F}}^2=P, \tag{2.4b}$$

$$|v_i|=1, \quad i=1,2,\cdots,K. \tag{2.4c}$$

The newly formulated problem in (2.4) is non-convex type because of the unimodular constraint on the phase shifts of the reflective RIS as given in (2.4c). This non-convex optimization problem can be efficiently solved by using the modified VAMP algorithm [27].

2.2   Solving the Joint Beamforming Problem through Optimization Oriented VAMP Algorithm

In this section, we briefly discuss solving the joint beamforming optimization problem for the reflective RIS through the optimization oriented VAMP algorithm [27]. Optimization oriented VAMP algorithm is the modified and extended version of the standard max-sum VAMP algorithm. The optimization oriented VAMP algorithm has two modules, namely: *i*) extended LMMSE module and *ii*) separable MAP projector

module. The LMMSE module optimizes the unconstrained objective function, while the constraints are applied by the projector module. The optimization-oriented VAMP algorithm is applied to jointly optimize the phase shifting vectors, $\boldsymbol{v}$, along with the precoding matrix $\mathbf{F}$. For this purpose, the formulated optimization problem in (2.4) is split into two sub-optimization tasks by using alternate minimization. As the phase shifting vectors, $\boldsymbol{v}$ are optimized by means of the modified VAMP algorithm inside a sub-optimization task, the precoding matrix $\mathbf{F}$ and the receive scaling factor α are optimized in the other task. The objective function for the optimization of the phase vector, $\boldsymbol{v}$ is expressed as:

$$\underset{\boldsymbol{v}}{\arg\min} \quad \left\|\alpha\mathbf{H}_{\text{s-u}}^{\mathsf{H}}\text{Diag}(\boldsymbol{v})\mathbf{H}_{\text{b-s}}\mathbf{F} - (\mathbf{I}_M - \alpha\mathbf{H}_{\text{b-u}}^{\mathsf{H}}\mathbf{F})\right\|_{\text{F}}^2 \tag{2.5a}$$

$$\text{s.t.} \quad |v_i| = 1 \quad i = 1, 2, \cdots, K. \tag{2.5b}$$

We reach the optimum solution by using the proposed optimization oriented VAMP algorithm. The algorithmic steps of the VAMP algorithm can be found in [27].

The objective function to optimize the precoding matrix, $\mathbf{F}$ and the receive scaling factor, α is expressed as:

$$\underset{\alpha,\mathbf{F}}{\arg\min} \left\|\alpha\left(\mathbf{H}_{\text{s-u}}^{\mathsf{H}}\text{Diag}(\widehat{\boldsymbol{v}}_{t-1})\mathbf{H}_{\text{b-s}} + \mathbf{H}_{\text{b-u}}^{\mathsf{H}}\right)\mathbf{F} - \mathbf{I}_M\right\|_{\text{F}}^2 + M\alpha^2\sigma_{\text{w}}^2 \tag{2.6a}$$

$$\text{s.t.} \quad \|\mathbf{F}\|_{\text{F}}^2 = P \tag{2.6b}$$

The sub-optimization problem in (2.6a) represents the constrained MMSE transmit precoding optimization for conventional MIMO systems [27]. It is solved in closed-form by jointly optimizing $\mathbf{F}$ and α using Lagrange optimization. Detailed solution of optimized $\mathbf{F}$ and α is given in Section 3.3.2.
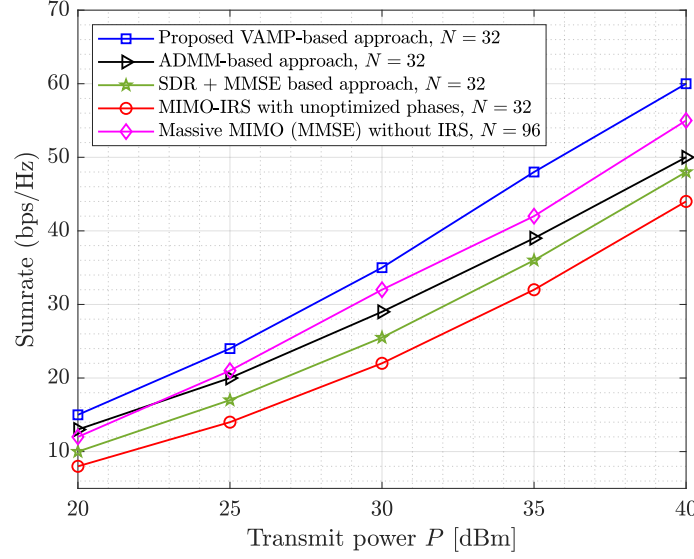
Figure 2.2: Sum-rate versus transmit power with $M = 8$ and $K = 256$. LOS components are present in the BS-RIS channels only [29].
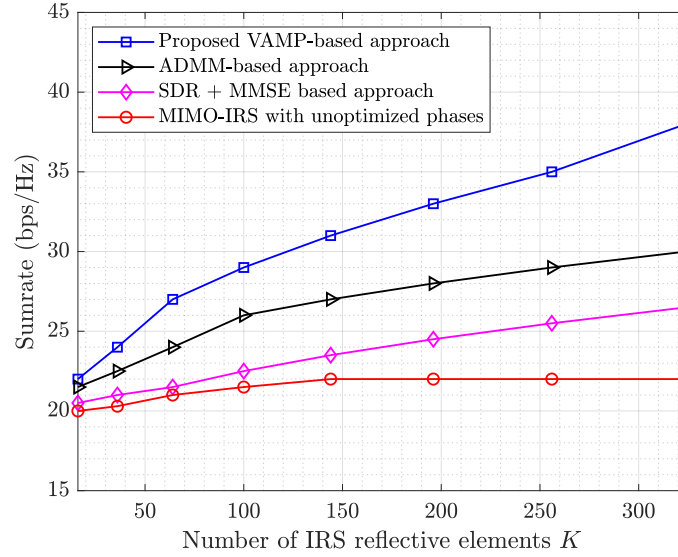
Figure 2.3: Sum-rate versus the number of reflective elements with $M = 8$, $N = 32$ and $P = 30$ dBm. LOS components are present in the BS-RIS channels only [29].

2.3 Numerical Results and Performance Analysis

In this section, performance of the reflective RIS in a multi-user MIMO communication setup is assessed, where the reflection coefficients are optimized using the optimization oriented VAMP algorithm. We consider a metric called the *sum-rate* [29] to compare the performance of the vamp-based approach with the state-of-the-art solutions i.e.: SDR-, ADMM- and massive MIMO-based approaches. The reflective RIS is placed to assist the BS to serve their intended users, where the users are situated at NLOS locations from the BS. We consider the BS to have 32 antennas and serving 8 users in the downlink. For comparison purpose, we also consider a massive MIMO scheme with 96 serving antennas at the BS. Fig. 2.2, illustrates the sum-rates versus the transmit power for the considered schemes. The reflective RIS, optimized with the optimization oriented VAMP algorithm, provides superior result to any other reflective RIS-based scheme. Even, the VAMP-based approach outperforms the massive MIMO scheme with relatively higher number of BS antennas. Fig. 2.3 depicts the sum-rates versus the number of reflective elements. For the VAMP-based approach, the achievable sum-rate with reflective RIS increases steadily with the number of reflective elements, as opposed to the unoptimized phases, where the sum-rate gets saturated at higher K. The VAMP-based approach also outperforms the SDR- and ADMM-based approaches in this scenario.

2.4 Summary

In this chapter, we reviewed the beamforming design of a reflective RIS-assisted multi-user MIMO system. A joint optimization problem has been formulated under the sum-MMSE criterion. The underlying optimization problem has been decomposed into two simpler sub-optimization tasks using the alternating minimization. The sub-tasks op-

timize the RIS phase shifts and the BS precoding matrix simultaneously. Regarding the phase shifts, a VAMP-based approach has been developed to solve the associated sub-optimization problem. The BS precoding matrix was obtained in closed-form using Lagrange optimization. Simulation results illustrate the superiority of the proposed approach over state-of-the-art solutions (e.g., the SDR-and ADMM-based approaches) in terms of achieved throughput.

Chapter 3

Lens-Type Redirective RIS for Single-cell MIMO Communication

RISs have recently drawn significant attention for their capability to enhance the spectral efficiency and coverage of wireless communication networks by smartly reconfiguring the wireless propagation environment. The conventional reflective RIS passively beamforms the incident signal by optimizing the phase shifts applied to the each reflective elements so as to achieve improved received power at end users without the help of any power amplifier. Interestingly, the control overhead and complexity of reflective RIS increases substantially with the number of reflective elements together with the control complexity [13]. In this chapter, we introduce the idea of using a lens-type redirective RIS (called RedRIS) which inherently relies on designing the beamforming vectors that redirect the incident wireless signals to the intended users. In the presence of a RedRIS, such beamforming vectors are selected among a DFT codebook that can scan all the directions of radiation [28]. We propose a general framework which involves the optimization of the back-to-back connections (or switching matrix) between the RedRIS ports instead of finding the optimal phase shifts in the purely reflective RIS.

The proposed switching mechanism drastically reduces the incurred signaling overhead and operational complexity for RIS-aided systems. In fact, the control overhead scales only logarithmically with the RedRIS size as opposed to the reflective RIS where the control overhead scales linearly with the number of antennas [14,15]. Although the lens-type RedRIS is a passive network element, it can be integrated with two-port amplifiers as opposed to the reflective RIS which would require reflection-mode amplifiers where achieving the stability becomes a major challenge [14,16].

We consider a lens-type RedRIS-aided wireless communication system serving multiple users in the downlink for both the single- and multi-cell settings. The lens-type RedRIS has a large number of antenna elements each of which with its dedicated port. Control of the RedRIS is achieved through back-to-back port switching connections which are optimized so as to wirelessly route the incoming signals to their intended users. We propose a dynamic solution that optimizes the switching matrix of the RedRIS ports for the single- and multi-cell scenarios. For the single-cell setup, we also optimize the active precoding matrix at the multi-antenna BS together with the receive scaling factor, while for the multi-cell setup with single-antenna BSs we only optimize the different receive scaling factors. The main contributions incorporated in this chapter are as follows:

- We consider the single-cell scenario and formulate a joint optimization problem for the design of the switching matrix at the lens-type RedRIS along with the BS precoding matrix and the receive scaling factor under the sum MMSE criterion. We do so by minimizing the received symbols error of all users thereby maximizing the overall spectral efficiency.

- We apply alternate optimization [33] to break the overall optimization problem into two sub-optimization tasks. One sub-problem consists in optimizing the BS precoding matrix and the receive scaling factor, while the other deals with the optimization of the ports switching matrix at the RedRIS.

- We find the optimum BS precoding matrix and the receive scaling factor in closed-form expressions using Lagrange optimization.

- To optimize the switching matrix, we develop an alternating optimization algorithm which consists of two modules: *i*) regularized least-squares (R-LS) module and *ii*) projection module.

- We also develop two methods to reduce the number of back-to-back connections between the RedRIS ports. In the first method, a small number of effective switches are selected for the multi-user scenario based on each user's MSE criterion. The second method is for the single-user scenario where the incident signal is redirected by connecting two RedRIS ports only. Such reduction in the number of port connections results in remarkable computational and control overhead savings compared to the fully-connected-ports configuration.

- We gauge the performance of the proposed schemes against the widely-studied reflective RIS-aided communication. The simulation results reveal that using a lens-type RedRIS with a limited number of effective port connections yields considerably higher throughput for both single- and multi-cell scenarios. Moreover, it will be seen that reducing the number of RedRIS back-to-back connections incurs a slight performance loss provided that the effective ports are appropriately selected as explained later on in this chapter. Finally, we test the robustness of the proposed solution by assessing its performance under residual channel estimation errors (i.e., imperfect CSI knowledge).

The rest of the chapter is organized as follows: the system model along with the assumptions and problem formulation are described in Section 3.1. In Section 3.2, we develop an algorithm for the joint optimization of the BS active precoding matrix and the receive scaling factor together with the ports switching matrix at the RedRIS. In

Section 3.3, the proposed algorithm is used to solve the joint optimization problem for the single-cell scenario and Section 3.4 discusses two methods for reducing the number of RedRIS port connections for the single- and multi-user cases. Simulation results are provided in Section 3.5 to illustrate the performance of the proposed RedRIS-based scheme.

3.1 System Model, Assumptions, and Problem Formulation

Consider a communication system consisting of one multi-antenna BS[1], a lens-type RedRIS, and M single-antenna users. The BS is equipped with N $(N > M)$ antenna elements. The lens-type RedRIS with K $(K > M)$ antenna ports is placed between the BS and the users to assist the communication. Based on CSI knowledge, back-to-back connections are established between appropriately selected combinations of unique pairs among the RedRIS ports. Fig. 3.1 illustrates the system model in which there exists a direct link between the BS and each m-th user, represented by a channel vector $\mathbf{h}_{\text{b-u},m} \in \mathbb{C}^N$. The channel vector for the link between the RedRIS and the m-th user is denoted as $\mathbf{h}_{\text{s-u},m} \in \mathbb{C}^K$. Let the MIMO channel between the BS and the RedRIS be denoted as $\mathbf{H}_{\text{b-s}} \in \mathbb{C}^{K \times N}$ with $\text{Rank}(\mathbf{H}_{\text{b-s}}) \geq M$. The incident signal at the lens-type RedRIS is redirected to the intended users owing to the refractive property of the lens and the reconfigured back-to-back connections of the antenna ports. The $K \times K$ switching matrix of the RedRIS ports is a symmetric permutation matrix denoted as $\boldsymbol{\Upsilon}$. A non-zero element υ_{ik} in $\boldsymbol{\Upsilon}$ means that ports i and k $(i \neq k)$ are back-to-back connected. We set the diagonal elements of $\boldsymbol{\Upsilon}$ to zero to avoid self-reflection on the

---

[1]For convenience, we focus in this section on the single-cell scenario. Extending the results to a multi-cell network will be done later on in Chapter 4
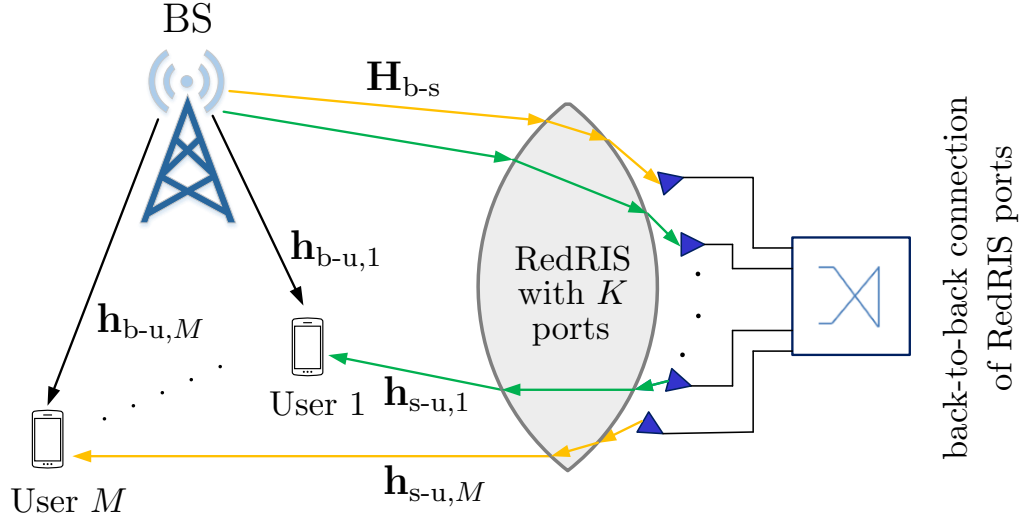
Figure 3.1: RedRIS-assisted multi-user MIMO system.

same RedRIS port. Being a Fourier plane, the lens performs spatial Fourier transform on both the incident and refracted signals. The signal received by the m-th user is thus expressed as follows:

$$\mathsf{y}_m \;=\; \mathbf{h}_{\text{s-u},m}^{\mathsf{H}} \mathbf{U}\boldsymbol{\Upsilon}\mathbf{U}\mathbf{H}_{\text{b-s}} \sum_{m'=1}^{M} \mathbf{f}_{m'}\mathsf{s}_{m'} \;+\; \mathbf{h}_{\text{b-u},m}^{\mathsf{H}} \sum_{m'=1}^{M} \mathbf{f}_{m'}\mathsf{s}_{m'} \;+\; \mathsf{w}_m \;,\;\; m=1,\dots,M. \quad (3.1)$$

Here, $\mathbf{U} \in \mathbb{C}^{K\times K}$ is the 2D DFT matrix obtained as the Kronecker product of a smaller dimension DFT matrix $\mathbf{U}_1 \in \mathbb{C}^{\sqrt{K}\times\sqrt{K}}$ with itself [37]:

$$\mathbf{U} = \mathbf{U}_1 \otimes \mathbf{U}_1.$$

Moreover, $\mathsf{s}_m \sim \mathcal{CN}(s_m; 0, 1)$ is the unknown transmitted symbol, $\mathsf{w}_m \sim \mathcal{CN}(w_m; 0, \sigma_{\text{w}}^2)$ is the additive white Gaussian noise (AWGN). Here, we assume the transmitted symbols

and the noise to have Gaussian distribution as we will be using Shannon's formula to calculate the sum-rate i.e.,

$$\widehat{C} \;=\; \sum_{m=1}^{M} \log_2 \left(1 + \text{SINR}_m\right). \quad m = 1, 2, \ldots, M, \tag{3.2}$$

where, SINR_m is the SINR of the m-th user. For complex Gaussian transmitted symbols, the I-MMSE relationship is given by [38]:

$$\text{MMSE}_m \;=\; \frac{1}{1 + \text{SINR}_m}. \tag{3.3}$$

Using the aforementioned I-MMSE relationship in (3.2), we obtain the sum-rate formula as:

$$\widehat{C} \;=\; \sum_{m=1}^{M} \log_2 \frac{1}{\text{MMSE}_m} \quad m = 1, 2, \ldots, M. \tag{3.4}$$

Besides, $\mathbf{f}_m \in \mathbb{C}^N$ for $m = 1, \ldots, M$ in (3.1) denote the active precoding vectors which are used for power allocation and beamforming purposes at the BS. Let P be the total transmit power and $\mathbf{F} = [\mathbf{f}_1, \mathbf{f}_2, \ldots, \mathbf{f}_M]$ be the overall precoding matrix. It follows that $\mathbb{E}\{\|\mathbf{Fs}\|_2^2\} = P$ with $\mathbf{s} = [\mathsf{s}_1, \mathsf{s}_2, \ldots, \mathsf{s}_M]^\mathsf{T}$ stacking the M unknown symbols transmitted by all the users. By further defining $\mathbf{y} \triangleq [\mathsf{y}_1, \mathsf{y}_2, \ldots, \mathsf{y}_M]^\mathsf{T}$, $\mathbf{w} \triangleq [\mathsf{w}_1, \mathsf{w}_2, \ldots, \mathsf{w}_M]^\mathsf{T}$, $\mathbf{H}_{\text{b-u}} \triangleq [\mathbf{h}_{\text{b-u},1}, \mathbf{h}_{\text{b-u},2}, \ldots, \mathbf{h}_{\text{b-u},M}]$, and $\mathbf{H}_{\text{s-u}} \triangleq [\mathbf{h}_{\text{s-u},1}, \mathbf{h}_{\text{s-u},2}, \ldots, \mathbf{h}_{\text{s-u},M}]$, then the input output relationship of the RedRIS-aided multi-user MIMO system is expressed in a compact matrix-vector form:

$$\mathbf{y} \;=\; \mathbf{H}_{\text{s-u}}^\mathsf{H} \mathbf{U} \boldsymbol{\Upsilon} \mathbf{U} \mathbf{H}_{\text{b-s}} \mathbf{Fs} + \mathbf{H}_{\text{b-u}}^\mathsf{H} \mathbf{Fs} + \mathbf{w}. \tag{3.5}$$

By denoting the overall effective channel matrix as:

$$\mathbf{H} \;\triangleq\; \mathbf{H}_{\text{s-u}}^\mathsf{H} \mathbf{U} \boldsymbol{\Upsilon} \mathbf{U} \mathbf{H}_{\text{b-s}} + \mathbf{H}_{\text{b-u}}^\mathsf{H}, \tag{3.6}$$

the signal received by all the users can be expressed in a more succinct form as follows:

$$\mathbf{y} \;=\; \mathbf{HFs} + \mathbf{w}. \tag{3.7}$$

The goal is to minimize the received symbols' errors of all users under the sum MMSE criterion. For a given MMSE on the received symbols, the spectral efficiency of the m-th user is lower-bounded by [38]:

$$C_m^{\text{MMSE}} = \log_2\left(\frac{1}{\text{MMSE}_m}\right), \quad m = 1, 2, \ldots, M. \tag{3.8}$$

We maximize the spectral efficiency of all users by jointly maximizing the M lower bounds in (3.8) or equivalently by minimizing the sum MMSE criterion as follows:

$$\underset{\alpha, \mathbf{F}, \mathbf{\Upsilon}}{\arg\min} \quad \mathbb{E}_{\mathbf{y},\mathbf{s}}\{\|\alpha\mathbf{y} - \mathbf{s}\|_2^2\}, \tag{3.9a}$$

$$\text{subject to} \quad \mathbb{E}_{\mathbf{s}}\{\|\mathbf{F}\mathbf{s}\|_2^2\} = P, \tag{3.9b}$$

$$\mathbf{\Upsilon} = \mathbf{\Upsilon}^{\mathsf{T}}, \tag{3.9c}$$

$$\mathbf{\Upsilon} \text{ is a permutation matrix,} \tag{3.9d}$$

$$\mathbf{\Upsilon}_{kk} = 0 \text{ for } k = 1, 2, \ldots, K. \tag{3.9e}$$

Here, $\alpha \in \mathbb{R}$ is the receive scaling factor [2] [35,36]. By recalling the expression of $\mathbf{y}$ in (3.5) and resorting to some algebraic manipulations, it can be shown that the optimization problem in (3.9) is equivalent to:

$$\underset{\alpha, \mathbf{F}, \mathbf{\Upsilon}}{\arg\min} \quad \left\|\alpha\mathbf{H}_{\text{s-u}}^{\mathsf{H}}\mathbf{U}\mathbf{\Upsilon}\mathbf{U}\mathbf{H}_{\text{b-s}}\mathbf{F} - (\mathbf{I}_M - \alpha\mathbf{H}_{\text{b-u}}^{\mathsf{H}}\mathbf{F})\right\|_{\text{F}}^2 + M\alpha^2\sigma_w^2, \tag{3.10a}$$

$$\text{subject to} \quad \{\|\mathbf{F}\|_{\text{F}}^2\} = P, \tag{3.10b}$$

$$\mathbf{\Upsilon} = \mathbf{\Upsilon}^{\mathsf{T}}, \tag{3.10c}$$

$$\mathbf{\Upsilon} \text{ is a permutation matrix,} \tag{3.10d}$$

$$\mathbf{\Upsilon}_{kk} = 0 \text{ for } k = 1, 2, \ldots, K. \tag{3.10e}$$

The optimization problem in (3.10) is non-convex due to the permutation constraint on $\mathbf{\Upsilon}$. We aim to solve it using an alternating minimization-based algorithm.

---

[2]Without loss of generality, α is taken to be real valued since any phase can be included in the precoding matrix $\mathbf{F}$.

3.2 Constrained Optimization of Symmetric Permutation Matrix

Let $\mathcal{P}_K = \{$*all possible symmetric permutation matrices of size* $K \times K\}$ and consider the related quadratic optimization problem:

$$\underset{\mathbf{X} \in \mathbb{R}^{K \times K}}{\arg\min} \qquad \|\mathbf{AXB} - \mathbf{Z}\|_{\mathrm{F}}^2, \tag{3.11a}$$

$$\text{subject to} \qquad \mathbf{X} = \mathbf{X}^{\mathsf{T}}, \tag{3.11b}$$

$$\mathbf{X} \text{ is a permutation matrix,} \tag{3.11c}$$

$$\mathbf{X}_{kk} = 0 \text{ for } k = 1, 2, \dots, K. \tag{3.11d}$$

in which the three matrices $\mathbf{A} \in \mathbb{C}^{M \times K}$, $\mathbf{B} \in \mathbb{C}^{K \times N}$, and $\mathbf{Z} \in \mathbb{C}^{M \times N}$ are known, while $\mathbf{X} \in \mathcal{P}_K$ is to be optimized. The underlying optimization problem is non-convex and will be solved by alternating between *i*) a regularized least-squares (R-LS) module that solves the unconstrained problem and *ii*) a projection module that enforces the constraints as shown in Fig. 3.2.

3.2.1 R-LS Module

Given an extrinsic update, $\bar{\mathbf{X}}$, from the projection module we consider the following regularized least-squares optimization problem:

$$\widetilde{\mathbf{X}}_{\mathrm{R\text{-}LS}} = \underset{\mathbf{X} \in \mathbb{R}^{K \times K}}{\arg\min} \qquad \|\mathbf{AXB} - \mathbf{Z}\|_{\mathrm{F}}^2 + \gamma_0 \|\mathbf{X} - \bar{\mathbf{X}}\|^2, \tag{3.12}$$

wherein γ_0 is a regularization parameter to be tuned. By vectorizing the cost function in 3.12 and defining $\mathbf{C} \triangleq (\mathbf{B}^{\mathsf{T}} \otimes \mathbf{A}) \in \mathbb{C}^{MN \times K^2}$ it follows that:

$$\widetilde{\mathbf{X}}_{\mathrm{R\text{-}LS}} = \mathrm{unvec}\left(\left(\mathbf{C}^{\mathsf{H}}\mathbf{C} + \gamma_0 \mathbf{I}_{K^2}\right)^{-1}\left(\mathbf{C}^{\mathsf{H}}\mathrm{vec}\left(\mathbf{Z}\right) + \gamma_0 \mathrm{vec}(\bar{\mathbf{X}})\right)\right). \tag{3.13}$$
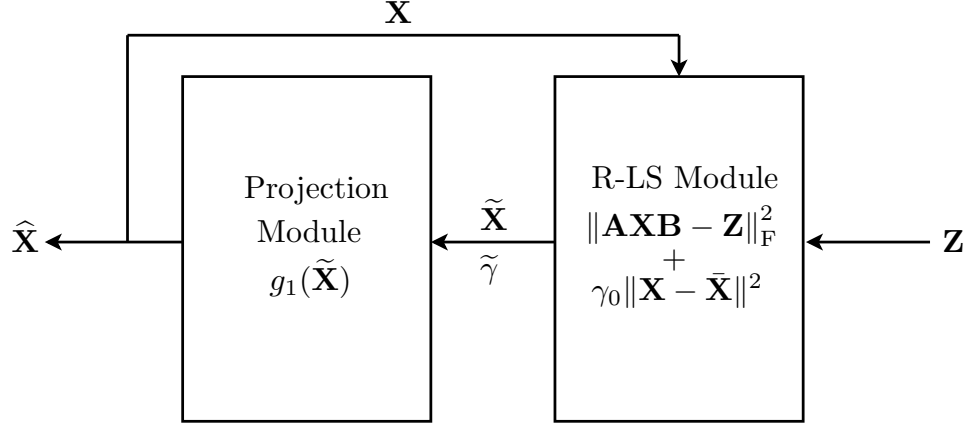
Figure 3.2: Block diagram of the proposed algorithm for symmetric permutation matrix optimization.

The associated precision is given by:

$$\widetilde{\gamma}_{\text{R-LS}} \;=\; \frac{K^2}{\text{tr}\left(\left(\mathbf{C}^{\mathsf{H}}\mathbf{C} + \gamma_0 \mathbf{I}_{K^2}\right)^{-1}\right)}, \tag{3.14}$$

from which one computes the extrinsic precision, $\widetilde{\gamma}$, that will be fed back to the projection module:

$$\widetilde{\gamma} \;=\; \widetilde{\gamma}_{\text{R-LS}} - \gamma_0. \tag{3.15}$$

The extrinsic update, $\widetilde{\mathbf{X}}$, that will be provided to the projection module is updated as follows:

$$\widetilde{\mathbf{X}} \;=\; \widetilde{\gamma}^{-1}\left(\widetilde{\gamma}_{\text{R-LS}}\widetilde{\mathbf{X}}_{\text{R-LS}} - \gamma_0\bar{\mathbf{X}}\right). \tag{3.16}$$

3.2.2 Projection Module

The projection module enforces the constraints by finding the nearest symmetric permutation matrix, $\widehat{\mathbf{X}}$, to the regularized least squares solution, $\widetilde{\mathbf{X}}$, i.e.:

$$\widehat{\mathbf{X}} \;=\; \underset{\mathbf{X} \in \mathcal{P}_K}{\arg\min} \; \left\| \widetilde{\mathbf{X}} - \mathbf{X} \right\|_{\mathrm{F}}^2 \;=\; \underset{\mathbf{X} \in \mathcal{P}_K}{\arg\max} \; \mathrm{Tr}(\mathbf{X}\Re\{\widetilde{\mathbf{X}}\}), \tag{3.17a}$$

$$\text{s.t.} \;\; \mathbf{X} = \mathbf{X}^{\mathsf{T}}, \tag{3.17b}$$

$$\mathbf{X}_{kk} = 0 \; \text{for} \; k = 1, 2, \ldots, K. \tag{3.17c}$$

The optimization in (3.17a) is an assignment-like problem which can be efficiently solved by using the Hungarian algorithm [39] with cubic complexity, i.e., $\mathcal{O}(K^3)$. For simplicity, however, we develop a simpler greedy approach that is shown in **Algorithm 1** where the objective function in (3.17a) is maximized sequentially. For convenience, in the sequel we use a shorthand notation for the projector function that obtains $\widehat{\mathbf{X}}$ from $\widetilde{\mathbf{X}}$ according to **Algorithm 1**, i.e.:

$$\widehat{\mathbf{X}} = g_1(\widetilde{\mathbf{X}}). \tag{3.18}$$

The extrinsic update $\bar{\mathbf{X}}$ that will be provided to the regularized least-square module is computed as follows:

$$\bar{\mathbf{X}} \;=\; \gamma_0^{-1} \left(\left[\gamma_0 + \widetilde{\gamma}\right]\widehat{\mathbf{X}} - \widetilde{\gamma}\widetilde{\mathbf{X}} \right). \tag{3.19}$$

The process of first finding $\widetilde{\mathbf{X}}$ and then projecting it on the set of symmetric permutation matrices, $\mathcal{P}_k$, so as to obtain $\widehat{\mathbf{X}}$ is repeated inside the algorithm until convergence. The block diagram and the algorithmic steps for the optimization framework are shown in Fig. 3.2 and summarized **Algorithm 2**, respectively.

3.3 Optimization of RedRIS-Aided Beamforming

In this section, we simultaneously optimize the ports switching matrix of the lens-type RedRIS, $\mathbf{\Upsilon}$, the BS precoding matrix, $\mathbf{F}$, and the receive scaling factor, α. The pro-

---

Algorithm 1 Greedy algorithm for the projection module

Given $\widetilde{\mathbf{X}} \in \mathbb{C}^{K \times K}$

1: $\widetilde{\mathbf{X}}^{(1)} = \widetilde{\mathbf{X}} - \text{Diag}(\widetilde{\mathbf{X}})$

2: Initialize $\mathcal{S} = \{(i,j) \mid i = 1, \ldots, K; \; j = 1, \ldots, K; \; i \neq j\}$ and $\widehat{\mathbf{X}} = \mathbf{0}_K$

3: **while** $\mathcal{S} \neq \varnothing$ **do**

4: $\quad (\widehat{i}, \widehat{j}) = \underset{(i,j) \in \mathcal{S}}{\arg \max} \; \Re\{\widetilde{\mathbf{X}}_{ij}^{(1)}\} + \Re\{\widetilde{\mathbf{X}}_{ji}^{(1)}\}$

5: $\quad \widehat{\mathbf{X}}_{\widehat{i}\widehat{j}} = 1, \widehat{\mathbf{X}}_{\widehat{j}\widehat{i}} = 1$

6: $\quad \mathcal{S} \leftarrow \mathcal{S} \setminus \{(i,j) \mid i = \widehat{i} \text{ or } j = \widehat{j}\}$

7: **end while**

8: **return** $\widehat{\mathbf{X}}$

---

posed framework alternates between **Algorithm 2** to find the optimal $\boldsymbol{\Upsilon}$ and Lagrange optimization to find the optimal $\mathbf{F}$ and α. To do so, we first split the joint optimization problem in (3.9) into two simpler sub-optimization tasks as follows:

$$\underset{\boldsymbol{\Upsilon}}{\arg \min} \qquad \mathbb{E}_{\mathbf{y},\mathbf{s}}\{\|\alpha \mathbf{y} - \mathbf{s}\|_2^2\}, \tag{3.20a}$$

$$\text{subject to} \qquad \boldsymbol{\Upsilon} = \boldsymbol{\Upsilon}^{\mathsf{T}}, \tag{3.20b}$$

$$\boldsymbol{\Upsilon} \text{ is a permutation matrix,} \tag{3.20c}$$

$$\boldsymbol{\Upsilon}_{kk} = 0 \text{ for } k = 1, 2, \ldots, K. \tag{3.20d}$$

$$\tag{3.20e}$$

$$\underset{\alpha, \mathbf{F}}{\arg \min} \qquad \mathbb{E}_{\mathbf{y},\mathbf{s}}\{\|\alpha \mathbf{y} - \mathbf{s}\|_2^2\}, \tag{3.21a}$$

$$\text{subject to} \qquad \mathbb{E}_{\mathbf{s}}\{\|\mathbf{F}\mathbf{s}\|_2^2\} = P. \tag{3.21b}$$

Algorithm 2 Algorithm for the optimization of symmetric permutation matrices

---

Given $\mathbf{A} \in \mathbb{C}^{M \times K}$, $\mathbf{B} \in \mathbb{C}^{K \times N}$, $\mathbf{Z} \in \mathbb{C}^{M \times N}$, required convergence precision (ϵ) and maximum number of iterations ($T_{\max}$)

1: Initialize $\bar{\mathbf{X}}_0$, $\gamma_0 \geq 0$ and $t \leftarrow 1$

2: **repeat**

3:      // R-LS Module.

4:      $\mathbf{C} = (\mathbf{B}^\mathsf{T} \otimes \mathbf{A})$

5:      $\widetilde{\mathbf{X}}_{\text{R-LS},t} = \text{unvec}\left(\left(\mathbf{C}^\mathsf{H}\mathbf{C} + \gamma_0 \mathbf{I}_{K^2} \right)^{-1} \left(\mathbf{C}^\mathsf{H}\text{vec}\left(\mathbf{Z}\right) + \gamma_0 \text{vec}(\bar{\mathbf{X}}_{t-1}) \right) \right)$

6:      $\widetilde{\gamma}_{\text{R-LS}} = \frac{K^2}{\text{tr}\left((\mathbf{C}^\mathsf{H}\mathbf{C} + \gamma_0 \mathbf{I}_{K^2})^{-1} \right)}$

7:      $\widetilde{\gamma} = \widetilde{\gamma}_{\text{R-LS}} - \gamma_0$

8:      $\widetilde{\mathbf{X}}_t = \widetilde{\gamma}^{-1} \left(\widetilde{\gamma}_{\text{R-LS}} \widetilde{\mathbf{X}}_{\text{R-LS},t} - \gamma_0 \bar{\mathbf{X}}_{t-1} \right)$

9:      // Projection Module.

10:     Compute projected matrix $\widehat{\mathbf{X}}_t = g_1(\widetilde{\mathbf{X}}_t)$ using **Algorithm 1**

11:     $\bar{\mathbf{X}}_t = \gamma_0^{-1} \left(\left[\gamma_0 + \widetilde{\gamma}\right] \widehat{\mathbf{X}}_t - \widetilde{\gamma}\widetilde{\mathbf{X}}_t \right)$

12:     $t \leftarrow t + 1$

13: **until** $\left\| \widehat{\mathbf{X}}_t - \widehat{\mathbf{X}}_{t-1} \right\|_\text{F}^2 \leq \epsilon \left\| \widehat{\mathbf{X}}_{t-1} \right\|_\text{F}^2$ or $t > T_{\max}$

14: **return** $\widehat{\mathbf{X}}_t$
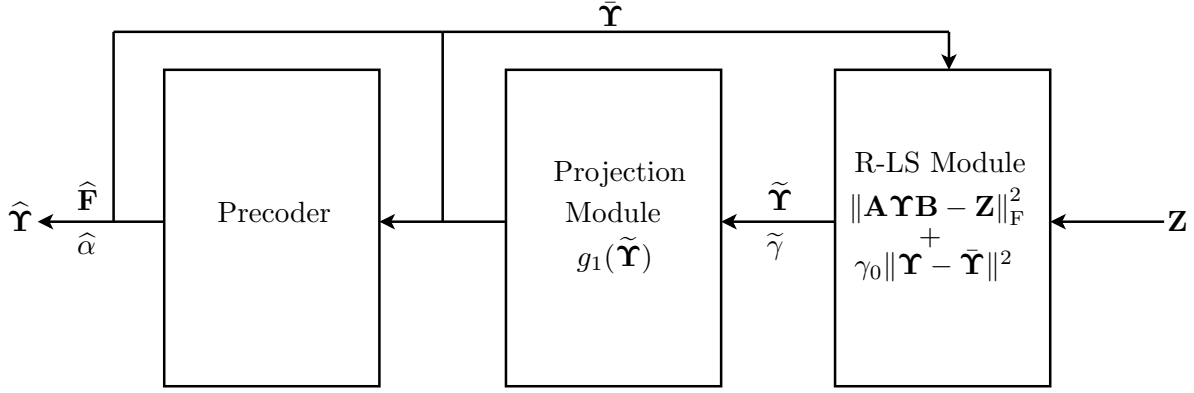
Figure 3.3: Block diagram of the proposed algorithm.

3.3.1 Finding the Optimal Switching Matrix of the RedRIS Ports

We use the R-LS and projection modules discussed in Section III to solve the sub-optimization problem in (3.20) which is explicitly re-stated as:

$$\underset{\mathbf{\Upsilon}}{\arg\min} \quad \left\| \alpha \mathbf{H}_{\text{s-u}}^{\mathsf{H}} \mathbf{U} \mathbf{\Upsilon} \mathbf{U} \mathbf{H}_{\text{b-s}} \mathbf{F} - (\mathbf{I}_M - \alpha \mathbf{H}_{\text{b-u}}^{\mathsf{H}} \mathbf{F}) \right\|_{\text{F}}^{2}, \tag{3.22a}$$

$$\text{subject to} \quad \mathbf{\Upsilon} = \mathbf{\Upsilon}^{\mathsf{T}}, \tag{3.22b}$$

$$\mathbf{\Upsilon} \text{ is a permutation matrix}, \tag{3.22c}$$

$$\mathbf{\Upsilon}_{kk} = 0 \text{ for } k = 1, 2, \ldots, K. \tag{3.22d}$$

We obtain the solution by substituting $\mathbf{A} = \alpha \mathbf{H}_{\text{s-u}}^{\mathsf{H}} \mathbf{U}$, $\mathbf{B} = \mathbf{U} \mathbf{H}_{\text{b-s}} \mathbf{F}$, and $\mathbf{Z} = \mathbf{I}_M - \alpha \mathbf{H}_{\text{b-u}}^{\mathsf{H}} \mathbf{F}$ in (3.11a) and solve for $\mathbf{X} = \mathbf{\Upsilon}$ using **Algorithm 2** in Section III.

3.3.2 Finding the Optimal BS Precoding Matrix and Receive Scaling Factor

The sub-optimization task in (3.21) is a constrained MMSE transmit precoding design problem for traditional MIMO systems which can be solved by jointly optimizing $\mathbf{F}$ and α using Lagrange optimization. The optimal α and $\mathbf{F}$ are obtained in closed-form expressions by following the same approach developed in [27]:

$$\widehat{\alpha} = g_2\left(\mathbf{H}\right) \triangleq \sqrt{\frac{1}{P}}\sqrt{\mathrm{Tr}\left(\left[\mathbf{H}^{\mathsf{H}}\mathbf{H} + \frac{M\sigma_{\mathrm{w}}^2}{P}\mathbf{I}_N\right]^{-2}\mathbf{H}^{\mathsf{H}}\mathbf{H}\right)}, \tag{3.23a}$$

$$\widehat{\mathbf{F}} = g_3\left(\mathbf{H}\right) \triangleq \frac{1}{\widehat{\alpha}}\left(\mathbf{H}^{\mathsf{H}}\mathbf{H} + \frac{M\sigma_{\mathrm{w}}^2}{P}\mathbf{I}_N\right)^{-1}\mathbf{H}^{\mathsf{H}}. \tag{3.23b}$$

A detailed description of the solution can be found in [35]. At this stage, the MSE at iteration t is given by:

$$E_t \triangleq \left\|\widehat{\alpha}_t(\mathbf{H}_{\mathrm{s\text{-}u}}^{\mathsf{H}}\mathbf{U}\widehat{\mathbf{\Upsilon}}_t\mathbf{U}\mathbf{H}_{\mathrm{b\text{-}s}} + \mathbf{H}_{\mathrm{b\text{-}u}}^{\mathsf{H}})\widehat{\mathbf{F}}_t - \mathbf{I}_M\right\|_{\mathrm{F}}^2 + M\widehat{\alpha}_t^2\sigma_{\mathrm{w}}^2. \tag{3.24}$$

The algorithm stops iterating when $|E_t - E_{t-1}| < \epsilon E_{t-1}$, where $\epsilon \in \mathbb{R}_+$ is some required convergence precision. The overall block diagram and the algorithmic steps are shown in Fig. 3.3 and **Algorithm 3**. The R-LS module of the algorithm can be efficiently implemented by exploiting the Kronecker matrix structure and singular value decomposition (SVD) [27].

3.4 Reducing the Number of Port Switchings

The dimension of the switching matrix, $\mathbf{\Upsilon}$, increases with the number of antenna ports in the lens-type RedRIS, resulting in an increased signaling overhead from the BS to the RedRIS. In this section, we propose two methods for reducing the number of connected ports down to N_p ($N_p \ll K$) ports while incurring a negligible degradation in overall performance. To reconfigure the switching matrix at the RedRIS, we need to assign

---

Algorithm 3 Alternating optimization of of $\mathbf{F}$, α and $\mathbf{\Upsilon}$

Given $\mathbf{H}_{\text{s-u}}$, $\mathbf{H}_{\text{b-u}}$, $\mathbf{H}_{\text{b-s}}$, $K \times K$ DFT matrix ($\mathbf{U}$), required convergence precision (ϵ), and maximum number of iterations ($T_{\max}$)

1: Initialize $\widehat{\mathbf{\Upsilon}}_0$, $\bar{\mathbf{\Upsilon}}_0$, $\gamma_0 \geq 0$ and $t \leftarrow 1$

2: $\widehat{\mathbf{H}}_0 = \mathbf{H}_{\text{s-u}}^{\mathsf{H}} \mathbf{U} \widehat{\mathbf{\Upsilon}}_0 \mathbf{U} \mathbf{H}_{\text{b-s}} + \mathbf{H}_{\text{b-u}}^{\mathsf{H}}$

3: $\widehat{\alpha}_0 = g_2\left(\widehat{\mathbf{H}}_0\right)$

4: $\widehat{\mathbf{F}}_0 = g_3\left(\widehat{\mathbf{H}}_0\right)$

5: **repeat**

6:     // R-LS Module.

7:     $\mathbf{A} = \widehat{\alpha}_{t-1} \mathbf{H}_{\text{s-u}}^{\mathsf{H}} \mathbf{U}$

8:     $\mathbf{B} = \mathbf{U} \mathbf{H}_{\text{b-s}} \widehat{\mathbf{F}}_{t-1}$.

9:     $\mathbf{Z} = \mathbf{I}_M - \widehat{\alpha}_{t-1} \mathbf{H}_{\text{b-u}}^{\mathsf{H}} \widehat{\mathbf{F}}_{t-1}$

10:     $\mathbf{C} = (\mathbf{B}^{\mathsf{T}} \otimes \mathbf{A})$

11:     $\widetilde{\mathbf{\Upsilon}}_{\text{R-LS},t} = \text{unvec}\left(\left(\mathbf{C}^{\mathsf{H}}\mathbf{C} + \gamma_0 \mathbf{I}_{K^2}\right)^{-1} \left(\mathbf{C}^{\mathsf{H}} \text{vec}\left(\mathbf{Z}\right) + \gamma_0 \text{vec}(\bar{\mathbf{\Upsilon}}_{t-1})\right)\right)$

12:     $\widetilde{\gamma}_{\text{R-LS}} = \frac{K^2}{\text{tr}\left((\mathbf{C}^{\mathsf{H}}\mathbf{C} + \gamma_0 \mathbf{I}_{K^2})^{-1}\right)}$

13:     $\widetilde{\gamma} = \widetilde{\gamma}_{\text{R-LS}} - \gamma_0$

14:     $\widetilde{\mathbf{\Upsilon}}_t = \widetilde{\gamma}^{-1}\left(\widetilde{\gamma}_{\text{R-LS}} \widetilde{\mathbf{\Upsilon}}_{\text{R-LS},t} - \gamma_0 \bar{\mathbf{\Upsilon}}_{t-1}\right)$

15:     // Projection Module.

16:     Compute projected matrix $\widehat{\mathbf{\Upsilon}}_t = g_1(\widetilde{\mathbf{\Upsilon}}_t)$ using **Algorithm 1**

17:     $\bar{\mathbf{\Upsilon}}_t = \gamma_0^{-1}\left(\left[\gamma_0 + \widetilde{\gamma}\right]\widehat{\mathbf{\Upsilon}}_t - \widetilde{\gamma}\widetilde{\mathbf{\Upsilon}}_t\right)$

18:     // Find the optimal α and $\mathbf{F}$.

19:     $\mathbf{H}_t = \mathbf{H}_{\text{s-u}}^{\mathsf{H}} \mathbf{U} \widehat{\mathbf{\Upsilon}}_t \mathbf{U} \mathbf{H}_{\text{b-s}} + \mathbf{H}_{\text{b-u}}^{\mathsf{H}}$

20:     $\widehat{\alpha}_t = g_2\left(\widehat{\mathbf{H}}_t\right)$

21:     $\widehat{\mathbf{F}}_t = g_3\left(\widehat{\mathbf{H}}_t\right)$

22:     $t \leftarrow t + 1$

23: **until** $|E_t - E_{t-1}| < \epsilon E_{t-1}$ or $t > T_{\max}$

24: **return** $\widehat{\mathbf{F}}_t$, $\widehat{\alpha}_t$, $\widehat{\mathbf{\Upsilon}}_t$.

$\log_2 K$ bits of indexing to every port connection. Therefore, the control overhead for the fully-connected RedRIS (i.e., K connected ports) is $K \log_2 K$. Whereas, with a reduced number of connected ports, $N_p/2$, the control overhead also decreases to $N_p \log_2 K$. So, the goal is to reduce the number of port switchings at the RedRIS and thereby lowering the incurred control overhead.

In a large-sized RedRIS, not all the beams in the incident wave are required to successfully reconstruct the signal at the receiver end, since the main beam and a few adjacent beams are usually sufficient to decode the transmitted information. The adjacent beams are required because of the leakage effect. This can be exploited to dynamically select the most significant ports so as to steer the RedRIS towards the dominant beams only. In this way, back-to-back connections are established between the selected antenna ports only while leaving the other ports disconnected. Reducing the number of the RedRIS ports connections significantly reduces the incurred control overhead and the overall complexity of the system. We propose the following two reduction approaches as outlined below.

3.4.1   Universal Reduction

In presence of a RedRIS with a large number, K, of antenna ports a large-size $K \times K$ switching matrix, $\mathbf{\Upsilon}$, establishes $K/2$ back-to-back port-connections. To obtain a reduced-size switching matrix, a small number of effective ports are selected to steer the lens-type RedRIS towards the dominant beams only. We use the MMSE criterion to determine the so-called effective RedRIS ports as follows. Let $\widehat{\mathbf{\Upsilon}}$ be the full optimal switching matrix returned by **Algorithm 3** and let $\mathcal{E}(\widehat{\mathbf{\Upsilon}})$ be the set of positions pertaining to all non-zero entries in $\widehat{\mathbf{\Upsilon}}$, i.e., $\mathcal{E}(\widehat{\mathbf{\Upsilon}}) = \left\{(i,j) | \widehat{\mathbf{\Upsilon}}_{ij} \neq 0, j < i \right\}$. Note that at this point $\left| \mathcal{E}(\widehat{\mathbf{\Upsilon}}) \right| = K$. For each $(i,j) \in \mathcal{E}(\widehat{\mathbf{\Upsilon}})$, we compute the MSE that results from setting the associated symmetric off-diagonal entries in $\widehat{\mathbf{\Upsilon}}$ to 0, i.e., $(\widehat{\mathbf{\Upsilon}}_{ij}, \widehat{\mathbf{\Upsilon}}_{ji}) = (0,0)$.

The smallest among the K computed MSEs corresponds to some position $(\widehat{i}, \widehat{j}) \in \mathcal{E}(\widehat{\mathbf{\Upsilon}})$. A reduced switching matrix, $\widehat{\mathbf{\Upsilon}}_1$, is obtained as follows:

$$\widehat{\mathbf{\Upsilon}}_1 = \widehat{\mathbf{\Upsilon}} - (\mathbf{e}_{\widehat{i}} \mathbf{e}_{\widehat{j}}^\top + \mathbf{e}_{\widehat{j}} \mathbf{e}_{\widehat{i}}^\top), \tag{3.25}$$

where $\mathbf{e}_k$ is the k-th canonical basis vector in $\mathbb{R}^K$, i.e., $\mathbf{e}_k$ has a single nonzero component which is equal to one at the k-th position. In plain English, the operation in (3.25) sets the symmetric entries in $\widehat{\mathbf{\Upsilon}}$ at positions $(\widehat{i}, \widehat{j})$ and $(\widehat{j}, \widehat{i})$ to zero. Since these positions correspond to the smallest incurred MSE, removing the associated back-to-back connection (by using $\widehat{\mathbf{\Upsilon}}_1$ instead of $\widehat{\mathbf{\Upsilon}}$) has the smallest impact on performance. The above-described reduction procedure is applied again to $\widehat{\mathbf{\Upsilon}}_1$ so as to remove the next least significant back-to-back connection and obtain another reduced switching matrix $\widehat{\mathbf{\Upsilon}}_2$. The process is repeated until at least $N_p \ll K$ effective ports are selected where $N_p/2$ is the number of paths in the BS-RIS channel. The algorithmic steps of the universal reduction method is shown in **Algorithm 4**.

Algorithm 4 Algorithm for universal reduction method

Given full optimal switching matrix $\widehat{\mathbf{\Upsilon}} \in \mathbb{R}^{K \times K}$, optimal $\widehat{\alpha}$, optimal $\widehat{\mathbf{F}}$, $\mathbf{H}_{\text{s-u}}$, $\mathbf{H}_{\text{b-u}}$, $\mathbf{H}_{\text{b-s}}$, $K \times K$ DFT matrix ($\mathbf{U}$), number of effective ports N_p

1: Initialize $t \leftarrow 0, \quad \widehat{\mathbf{\Upsilon}}_0 = \widehat{\mathbf{\Upsilon}}$

2: **repeat**

3: $\quad (\widehat{i}, \widehat{j}) = \underset{(i,j) \in \mathcal{E}(\widehat{\mathbf{\Upsilon}}_t)}{\arg\min} \left\| \widehat{\alpha}(\mathbf{H}_{\text{s-u}}^{\mathsf{H}} \mathbf{U} \widehat{\mathbf{\Upsilon}}_t \mathbf{U} \mathbf{H}_{\text{b-s}} + \mathbf{H}_{\text{b-u}}^{\mathsf{H}}) \widehat{\mathbf{F}} - \mathbf{I}_M \right\|_{\text{F}}^2, \quad \text{s.t.} \quad [\widehat{\mathbf{\Upsilon}}_t]_{ij} \leftarrow 0,$
$\quad [\widehat{\mathbf{\Upsilon}}_t]_{ji} \leftarrow 0$

4: $\quad \widehat{\mathbf{\Upsilon}}_t = \widehat{\mathbf{\Upsilon}}_{t-1} - (\mathbf{e}_{\widehat{i}} \mathbf{e}_{\widehat{j}}^\top + \mathbf{e}_{\widehat{j}} \mathbf{e}_{\widehat{i}}^\top)$

5: $\quad t \leftarrow t + 1$

6: **until** $\text{Rank}(\mathbf{\Upsilon}_{\text{t}}) = N_p$

7: **return** $\widehat{\mathbf{\Upsilon}}_t$.

3.4.2 Two-Port Solution for the Single-User Case

For the single-user case ($M = 1$), an efficient approach — referred to as "two-port solution" — that uses only $N_p = 2$ effective ports at the RedRIS is proposed. The two-port solution is obtained in a closed-form by determining the two antenna elements that capture most of the energy in the cascaded BS-RedRIS-user channel. By letting $\mathbf{H}^{(1)} = \mathbf{U}\mathbf{H}_{\text{b-s}} \in \mathbb{C}^{K \times N}$ and $\mathbf{h}^{(2)} = \mathbf{h}_{\text{s-u}}\mathbf{U} \in \mathbb{C}^{1 \times K}$, then the antenna-wise captured energies in the BS-RedRIS channels ($\mathbf{e}_{\text{b-s}}$), and the user-RedRIS channels ($\mathbf{e}_{\text{s-u}}$) are defined respectively as:

$$e_{\text{b-s},i} = \sum_{n=1}^{N} \left| \mathbf{H}^{(1)}_{in} \right|^2, \ i = 1, \dots, K, \tag{3.26}$$

$$e_{\text{s-u},j} = \left| \mathbf{h}^{(2)}_{j} \right|^2, \ \ j = 1, \dots, K. \tag{3.27}$$

The objective function for finding the optimum port index $(\widehat{i}, \widehat{j})$ for the two-port solution is expressed as follows:

$$\widehat{i} = \arg\max_{1 \leq i \leq K} \ e_{\text{b-s},i}. \tag{3.28a}$$

$$\widehat{j} = \arg\max_{1 \leq j \leq K} \ e_{\text{s-u},j}. \tag{3.28b}$$

3.5 Numerical Results and Performance Analysis

In this section, we present the performance of the proposed RedRIS-aided communication schemes by means of Monte-Carlo simulations and using the *sum-rate* as a performance metric. Given the MMSE of the received symbol pertaining to each m-th user, the sum-rate of the overall system is expressed as:

$$\widehat{C} = \sum_{m=1}^{M} \log_2 \left(\frac{1}{\text{MMSE}_m} \right). \tag{3.29}$$

In the single-cell scenario, we assume that the RedRIS is situated at a fixed distance $d_{\text{RIS}} = 500$ m from the BS while in the multi-cell setup the BSs are located at a uniform

radial distance of 100 m to 500 m from the RedRIS. In both scenarios, the users are uniformly spread at a distance ranging from 10 m to 50 m from the RedRIS. We assume there are $Q_{\mathrm{RIS}} = 10$ multi-path components in the BS-RedRIS channel and $Q_{\mathrm{b\text{-}u}} = 2$ multi-path components in each BS-user channel. We also assume that the N antenna elements at the BS and the K antenna elements at the RedRIS (connected through their respective ports) are arranged in square uniform planar arrays. We use the parametric

Table 3.1: Simulation parameters with the notations and values.

Parameter	Notation, Value	Parameter	Notation, Value
Multi-paths in the BS-RIS channel	$Q_{\mathrm{RIS}} = 10$	Channel path gain	$c_q \sim$ $\mathcal{CN}(0,1)$
Multi-paths in the BS-user channel	$Q_{\mathrm{b\text{-}u}} = 2$	Distance between BS and RIS	$d_{\mathrm{RIS}} \in$ $[100, 500]$ m
Multi-paths in the RIS-user channel	$Q_{\mathrm{s\text{-}u}} = 2$	Distance between RIS and users	$d' \in [10, 50]$ m
Path-loss exponent of the RIS-user channel	$\eta = 2.5$	Noise variance	$\sigma_{\mathrm{w}}^2 = -100$ dBm
Path-loss exponent of the RIS-BS channel	$\eta = 2.5$	Reference distance	$d_0 = 1$ m
Path-loss exponent of the BS-user channel	$\eta = 3.7$	Path-loss at reference distance	$C_0 = -30$ dB

or path-based channel model to generate the channel matrices [38]. We refer the reader to [27] for more details on the considered channel model and corresponding parameters. The simulation parameters are listed in Table 3.1.

We also consider two line-of-sight (LOS) conditions. In the first case, we assume only the BS-RedRIS channel has a LOS component. In the second case, we assume both the BS-RedRIS and RedRIS-user channels have LOS components, but there is no LOS component in the BS-user channels. We gauge the performance of the propose schemes against:

1. A MIMO system assisted by one reflective RIS with optimized phase shifts and the MMSE precoding at the BS.

2. A MIMO system assisted by one RedRIS with an unoptimized (i.e., random) switching matrix and MMSE precoding at the BS.

3.5.1   Simulation Results with Perfect CSI

Only BS-RIS channel has a LOS component

This situation is commonly encountered in typical urban areas where the BS is usually situated at a distant location from the users and has no direct link to them due to blockage [27]. We consider a 32-antennas BS that is serving 4 users. Fig. 3.4 illustrates the achievable sum-rate versus the total transmit power P. It is observed that the optimized fully-connected RedRIS provides a higher sum-rate than the optimized reflective RIS for all transmit powers. We also observe that the optimized partially-connected RedRIS with $N_p = 20$ effective ports (selected via the reduction method developed in Section 3.4) achieves almost the same sum-rate as the fully-connected RedRIS. The former does so while incurring much less control overhead and operational complexity.

Fig. 3.5 shows a plot of the sum-rate against the total transmit power for the single-user scenario. It is observed that the sum-rates for the different schemes follow a similar trend to that of the multi-user case. Here, the achievable sum-rates of both the partially-and fully-connected RedRIS are almost as good as the sum-rate of the reflective RIS
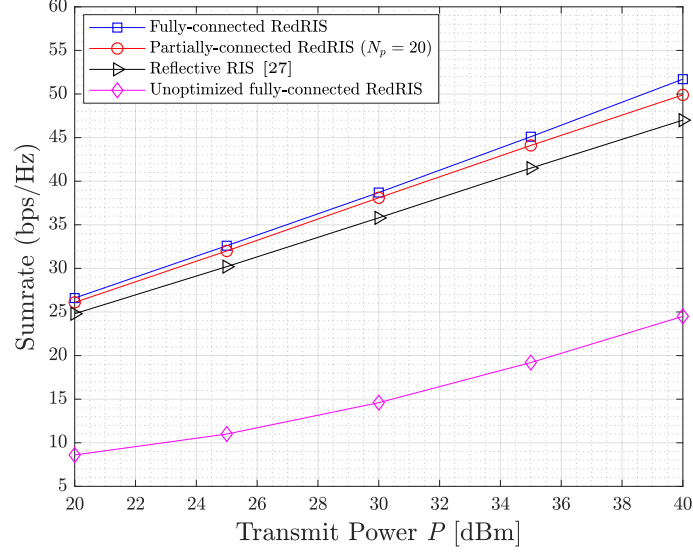
Figure 3.4: Sum-rate versus transmit power with $M = 4$ and $K = 256$. LOS component is present in the BS-RIS channel only.
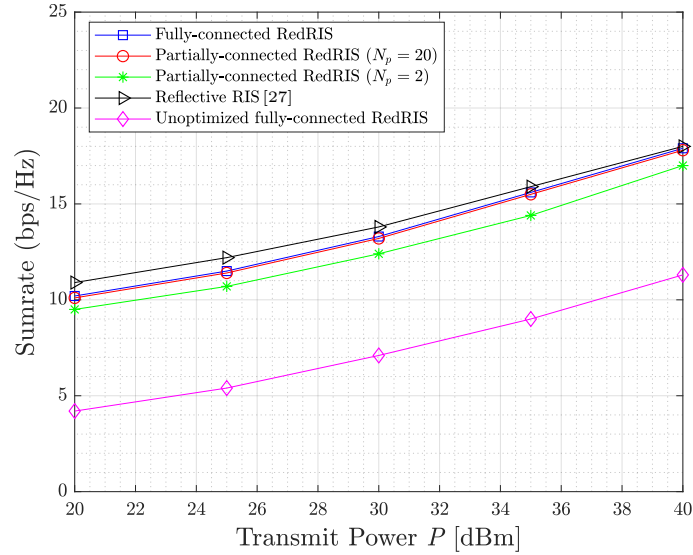

Figure 3.5: Sum-rate versus transmit power with $M = 1$ and $K = 256$. LOS component is present in the BS-RIS channel only.
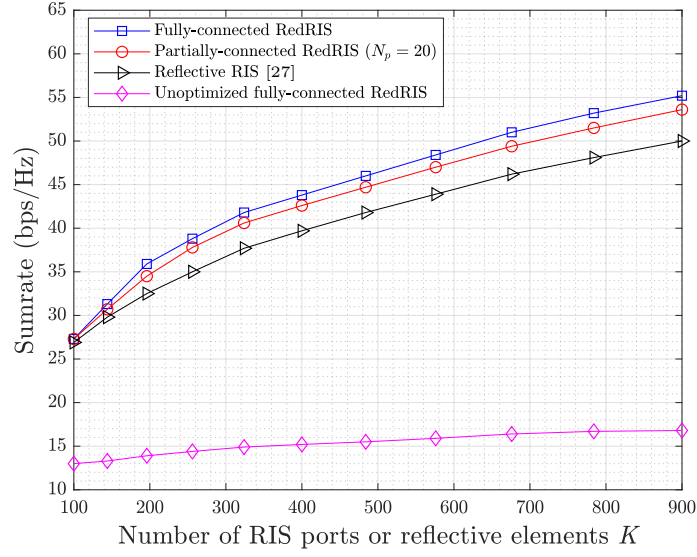
Figure 3.6: Sum-rate versus the number of RedRIS ports or reflection elements with $M = 4$, $N = 32$, and $P = 30$ dBm. LOS component is present in the BS-RIS channel only.
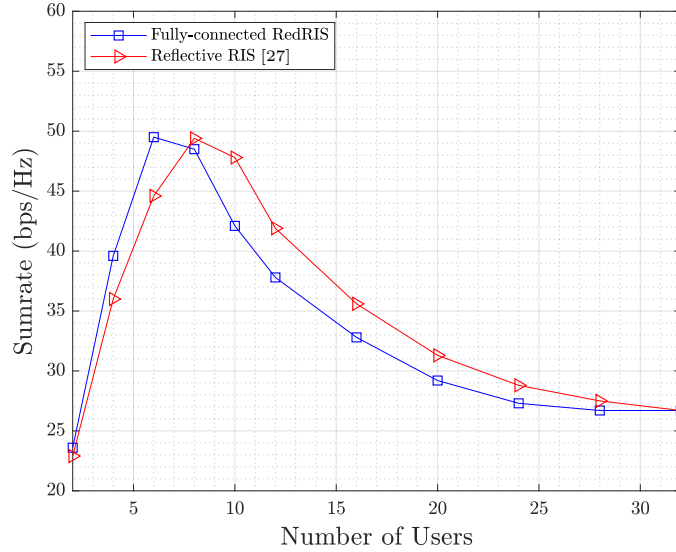
Figure 3.7: Sum-rate versus number of users with $N = 32$, $K = 256$, and $P = 30$ dBm. LOS component is present in the BS-RIS channel only.

with optimized reflection coefficients. It should be noted, however, that optimizing the phase shifts of the reflective RIS for the single-user case is much easier than the multi-user case. This is due to the conflicting requirements between the different users in the latter case thereby resulting in a sub-optimum total sum-rate. RedRIS overcomes this problem by redirecting the incident signals towards the intended users with no conflicting requirements thereby resulting in a much higher total sum-rate as seen in Fig. 3.5. Besides, the RedRIS with a two-port connection (selected by the reduction method developed in Section 3.4) also attains a sum-rate close to the other schemes. In the single-user case, it is possible to achieve a higher sum-rate using a single connection between the aptly selected two ports, since there is only one dominant path that needs to be captured and redirected by the RedRIS.

Fig. 3.6 depicts the sum-rate against the number, K, of ports (in RedRIS) or reflection elements (in reflective RIS) at 30 dBm transmit power. As expected, the sum-rate increases steadily with K. Although the sum-rate at small values of K is the same for all schemes, a significant gap is observed as K increases. It is also seen that the optimized partially-connected RedRIS with only $N_p = 20$ selected ports performs as good as the fully-connected RedRIS, with the advantage of less complexity and control overhead.

Fig. 3.7 depicts the sum-rate against the number of users. As seen there, the sum-rate increases with the number of users up to certain point beyond which it declines drastically. In fact, in the single-cell scenario, the maximum number of users that the RedRIS-aided system can support is given by the number of multi-path components in the BS-RedRIS channel under the assumption that the number of BS antennas are higher than the number of the aforementioned multi-path components. Here, we have considered $Q_{\mathrm{RIS}} = 10$ multi-path components in the BS-RedRIS channel, and $N = 32$ ($N > Q_{\mathrm{RIS}}$) BS antennas. So this particular RedRIS-assisted system can support maximum 10 users without any impact in the performance. The sum-rate starts
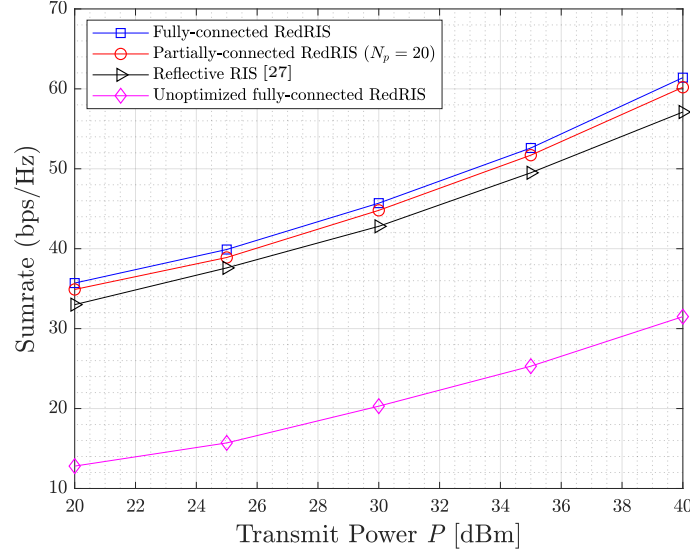
Figure 3.8: Sum-rate versus transmit power with $M = 4$ and $K = 256$. LOS components are present in both the BS-RIS channel and the RIS-users channels.

declining when the number of users exceeds 10 in the network. Besides, The sum-rate achieved with a fully-connected RedRIS follows the same trend as the reflective RIS, although there is a performance gap for higher number of users.

BS-RIS channel and RIS-user channels have LOS components

Figs. 3.8 and 3.9 depict the sum-rate performance versus the transmit power for multi- and single-user cases, respectively. As expected, it is observed that the presence of LOS components in the RIS-users channels improves the sum-rate appreciably in both scenarios. Fig. 3.10 shows the sum-rate against the number of ports (or reflection elements) in presence of a LOS component which is an upwardly shifted version of the graph for the NLOS scenario due to the improved sum-rate.
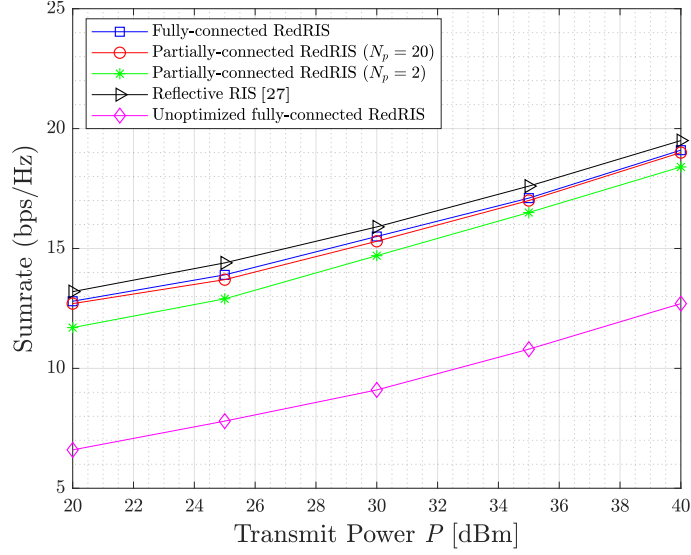
Figure 3.9: Sum-rate versus transmit power with $M = 1$ and $K = 256$. LOS components are present in both the BS-RIS channel and the RIS-users channels.
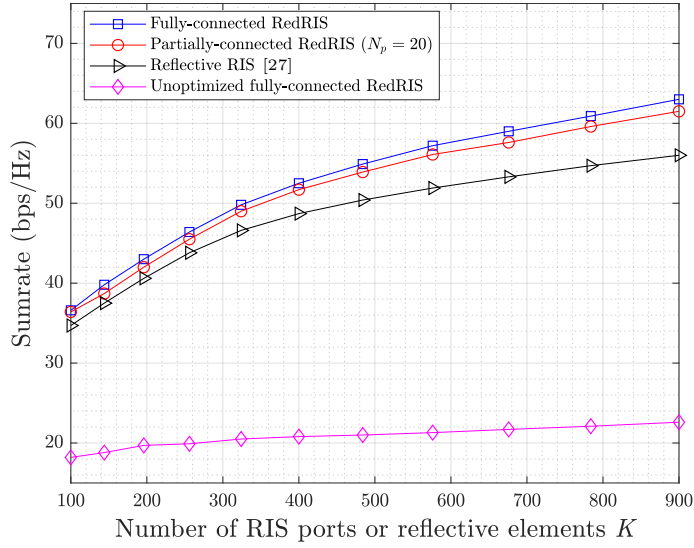

Figure 3.10: Sum-rate versus the number of RIS ports or reflection elements with $M = 4$, $N = 32$, and $P = 30$ dBm. LOS components are present in both the BS-RIS channel and the RIS-users channels.
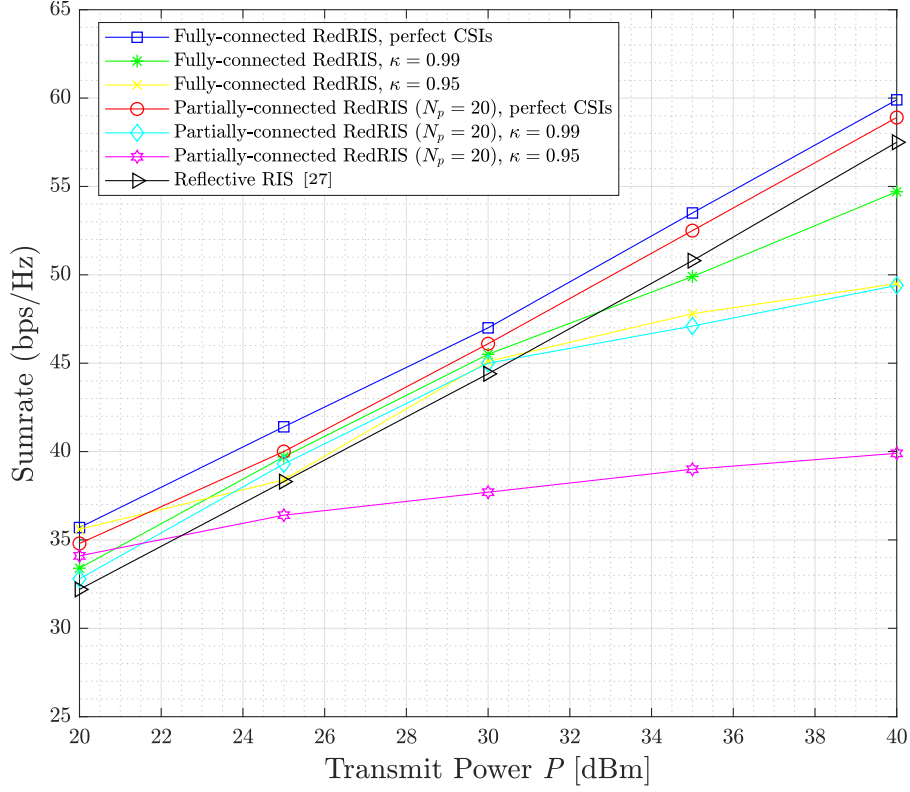
Figure 3.11: Sum-rate versus transmit power under imperfect CSI ($M = 4$, $N = 32$ and $K = 256$). LOS components are present in both the BS-RIS channel and the RIS-users channels.

3.5.2 Simulation Results with Imperfect CSI

In this section, we assess the performance of RedRIS-aided communication in presence of residual channel estimation errors. We refer the reader to [27] for the further details on how the latter are modeled and we exhibit the corresponding results in Fig. 3.11. For comparison purposes, we also show the sum-rate curves under perfect CSI. In presence of small residual channel estimation errors, i.e., at $\kappa = 0.99$ and at low SNRs, both of the fully- and partially-connected RedRIS yield almost the same sum-rate as in the perfect CSI case. Moreover, at low SNRs and $\kappa = 0.99$, RedRIS outperforms the reflective RIS

even with perfect CSI knowledge. However, at higher channel estimation errors (i.e., with $\kappa = 0.95$) and low SNRs, the sum-rate of the fully-connected RedRIS remains unaffected as opposed to the partially-connected RedRIS which incurs a significant loss. Such performance degradation is caused by the induced errors in selecting the significant ports due to the imperfect CSI knowledge. In the case of fully-connected RedRIS, the proposed solution is highly resilient to imperfect CSI condition and outperforms by far the conventional reflective RIS-based solution.

3.6   Summary

In this chapter, we propse the idea of using a lens-type redirective surface (called RedRIS) in multi-user MIMO communication and developed a dedicated algorithm to optimize the ports switching matrix. To that end, we first formulated a joint optimization problem to maximize the spectral efficiency of the users by minimizing the sum MMSE of all users' received symbols in the single-cell scenario. The joint optimization problem consists of two sub-optimization tasks: i) the receive scaling factor and the precoding matrix at the BS were optimized in closed form using Lagrange optimization, while ii) the switching matrix of the RedRIS ports was optimized iteratively using alternating optimization. We then proposed two methods for reducing the number of effective port connections in the RedRIS so as to reduce the control overhead and computational complexity. The simulation results reveal that the proposed RedRIS-based solution, even with a reduced number of port connections, performs better than the widely-studied reflective RIS solution. Moreover, the resilience of RedRIS against residual channel estimation errors was validated empirically.

Chapter 4

Redirective RIS for Multi-cell Interference Channels

In Chapter 3, we proposed an idea of using a lens-type redirective RIS (called RedRIS) to assist the multi-user MIMO communication in a single-cell network. In this chapter, we extend the framework to the multi-cell scenario (wherein each cell is equipped with a single-antenna BS and each BS is serving one user at a time) and jointly optimize the switching matrix of the RedRIS and the different receive scaling factors by means of **Algorithm 3**. The main contributions incorporated in this chapter are as follows:

- We consider a multi-cell scenario and formulate a joint optimization problem for the design of the switching matrix at the lens-type RedRIS along with the different receive scaling factors under the sum MMSE criterion. We do so by minimizing the received symbol error of all users thereby maximizing the overall spectral efficiency.

- We jointly optimize the switching matrix and the receive scaling factors by means of a modified version of **Algorithm 3**.

- We find the different receive scaling factors in closed-form expression.

- Finally, we gauge the performance of the proposed multi-cell scheme against the conventional reflective RIS-aided schemes. The simulation results replicate the single-cell scenario i.e.: using a lens-type RedRIS with a limited number of effective port connections yields considerably higher throughput than the reflective RIS.

The rest of the chapter is organized as follows: the system model along with the assumptions and problem formulation are described in Section 4.1. In Section 4.2, we jointly optimize the switching matrix and the receive scaling factors by means of a modified version of the proposed algorithm. Simulation results are provided in Section 4.3 to illustrate the performance of the proposed RedRIS-based scheme in a multi-cell network.

4.1 System Model, Assumptions, and Problem Formulation

In this section, we extend the system to an M-cell network where each cell is equipped with a single-antenna BS and each BS is serving one user at a time. A RedRIS with K ($K > M$) antenna ports is simultaneously assisting all the BSs to serve their intended users. Similar to the single-cell scenario, back-to-back connections are established between the the RedRIS antenna ports to facilitate the communication. For simplicity, representation of the channel vectors is the same as in the single-cell setup (see Section II) and Fig. 4.1 illustrates the system model for the multi-cell scenario. The input-output relationship for the RedRIS-aided multi-cell system is expressed as:

$$\mathbf{y} = \mathbf{H}_{\text{s-u}}^{\mathsf{H}} \mathbf{U} \boldsymbol{\Upsilon} \mathbf{U} \mathbf{H}_{\text{b-s}} \mathbf{s} + \mathbf{H}_{\text{b-u}}^{\mathsf{H}} \mathbf{s} + \mathbf{w}. \tag{4.1}$$
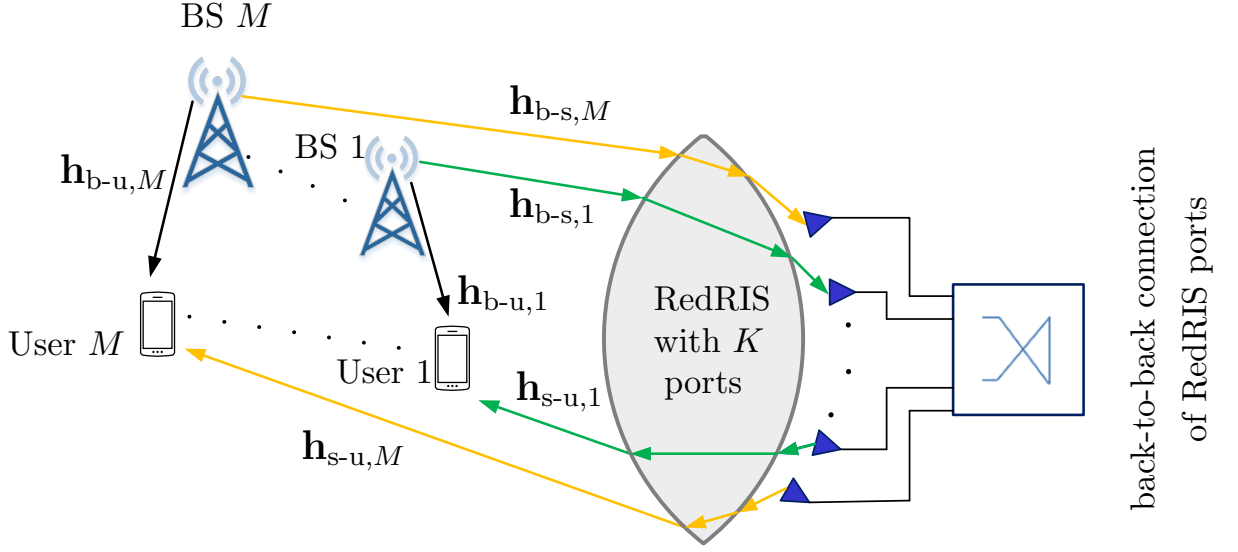
Figure 4.1: RedRIS-assisted communication scheme for multi-cell system.

Here, $\mathbf{H}_{\text{s-u}} \in \mathbb{C}^{K \times M}$, $\mathbf{H}_{\text{b-s}} \in \mathbb{C}^{K \times M}$ and $\mathbf{H}_{\text{b-u}} \in \mathbb{C}^{M \times M}$ are the related channel matrices. In (4.1), no BS precoding matrix ($\mathbf{F}$) is required as opposed to the single-cell case. This is because there is no joint processing between the BSs and every BS is serving its own user only. We formulate the objective function for the multi-cell scenario under the sum MMSE criterion as follows:

$$\arg\min_{\boldsymbol{\alpha},\boldsymbol{\Upsilon}} \qquad \mathbb{E}_{\mathbf{y},\mathbf{s}}\{\|\text{Diag}(\boldsymbol{\alpha})\mathbf{y} - \mathbf{s}\|_2^2\}, \tag{4.2a}$$

$$\text{subject to} \qquad \boldsymbol{\Upsilon} = \boldsymbol{\Upsilon}^{\mathsf{T}}, \tag{4.2b}$$

$$\boldsymbol{\Upsilon} \text{ is a permutation matrix}, \tag{4.2c}$$

$$\boldsymbol{\Upsilon}_{kk} = 0 \text{ for } k = 1, 2, \ldots, K. \tag{4.2d}$$

Here, $\boldsymbol{\alpha} \in \mathbb{C}^M$ is a vector that contains the receive scaling factors of all users. By recalling the expression of $\mathbf{y}$ in (4.1) and resorting to some algebraic manipulations, the

objective function in (4.2) is re-written as:

$$\underset{\boldsymbol{\alpha},\boldsymbol{\Upsilon}}{\arg\min} \quad \left\|\mathrm{Diag}(\boldsymbol{\alpha})\mathbf{H}_{\text{s-u}}^{\mathsf{H}}\mathbf{U}\boldsymbol{\Upsilon}\mathbf{U}\mathbf{H}_{\text{b-s}} - (\mathbf{I}_M - \mathrm{Diag}(\boldsymbol{\alpha})\mathbf{H}_{\text{b-u}}^{\mathsf{H}})\right\|_{\mathrm{F}}^2 + \|\boldsymbol{\alpha}\|^2\sigma_w^2, \quad (4.3a)$$

$$\text{subject to} \quad \boldsymbol{\Upsilon} = \boldsymbol{\Upsilon}^{\mathsf{T}}, \quad (4.3b)$$

$$\boldsymbol{\Upsilon} \text{ is a permutation matrix,} \quad (4.3c)$$

$$\boldsymbol{\Upsilon}_{kk} = 0 \text{ for } k = 1, 2, \ldots, K. \quad (4.3d)$$

4.2 Joint Optimization for the Multiple Single-Antenna BS system

The optimization problem in (4.3) is non-convex and will also be solved by means of **Algorithm 3** developed in Section 3.2. For a fixed $\boldsymbol{\alpha}$, we replace $\mathbf{A} = \mathrm{Diag}(\boldsymbol{\alpha})\mathbf{H}_{\text{s-u}}^{\mathsf{H}}\mathbf{U}$, $\mathbf{B} = \mathbf{U}\mathbf{H}_{\text{b-s}}$, and $\mathbf{Z} = \mathbf{I}_M - \mathrm{Diag}(\boldsymbol{\alpha})\mathbf{H}_{\text{b-u}}^{\mathsf{H}}$ in (3.11a) and solve for $\mathbf{X} = \boldsymbol{\Upsilon}$ by using **Algorithm 3**. To find the optimal vector of receive scaling factors, $\boldsymbol{\alpha}$, we minimize the individual users' MSEs under the MMSE criterion as:

$$\min_{\alpha_m \in \mathbb{C}} \mathbb{E}\left\{|\alpha_m(\mathbf{h}_{\text{s-u,m}}^{\mathsf{H}}\mathbf{U}\boldsymbol{\Upsilon}\mathbf{U}\mathbf{H}_{\text{b-s}}\mathbf{s} + \mathsf{w}_m) - \mathsf{s}_m|^2\right\}. \quad (4.4)$$

After taking expectation with respect to $\mathbf{s}$ and w_m, (4.4) reduces simply to:

$$\min_{\alpha_m \in \mathbb{C}} \|\alpha_m^*\mathbf{v} - \mathbf{e}_m\|_2^2 + \sigma_w^2|\alpha_m|^2, \quad (4.5)$$

wherein $\mathbf{v} \triangleq \mathbf{H}_{\text{b-s}}^{\mathsf{H}}\mathbf{U}^{\mathsf{H}}\boldsymbol{\Upsilon}\mathbf{U}^{\mathsf{H}}\mathbf{h}_{\text{s-u,m}} \in \mathbb{C}^M$ and $\mathbf{e}_m$ is the m-th canonical basis vector in $\mathbb{R}^M$, i.e., $\mathbf{e}_m$ has a single nonzero component which is equal to one at the m-th position. Then, by setting the derivative of the cost function in (4.5) with respect to α_m to zero and solving for α, we obtain the optimum receive scaling factor for each m-th user as:

$$\alpha_m^{\text{opt}} = \frac{\mathbf{v}^{\mathsf{H}}\mathbf{e}_m}{\|\mathbf{v}\|^2 + \sigma_w^2}. \quad (4.6)$$

The number of back-to-back connections of the RedRIS ports can be reduced by applying the approach developed in Section 3.4 (i.e., **Algorithm 4**) for further overhead savings.

4.3   Numerical Results and Performance Analysis

In this section, we present the performance of the RedRIS in a multi-cell network by assessing the simulation-based results. We consider a system consisting of 8 cells each of which being equipped with a single-antenna BS and each BS is serving one user at a time with the help of the RedRIS. We assume that the BSs are located at a uniform radial distance of 100 m to 500 m from the RedRIS. We also consider that the users are uniformly spread at a distance ranging from 10 m to 50 m from the RedRIS. We assume 10 multi-path components in the BS-RedRIS channel and 2 multi-path components in each BS-user channel. We also assume that the N antenna elements at the BS, and the K antenna elements at the RedRIS (connected through their respective ports) are arranged in square uniform planar arrays. In the multi-cell scenario, the maximum number of users that the RedRIS-aided system can support is given by the maximum number of port connections, i.e., $(K/2)$. Here we consider the same channel model and parameters as in the single-cell configuration we already mentioned in Table 3.1.

4.3.1   Simulation Results with Perfect CSI

Fig. 4.2 compares the achieved sum-rate of the RedRIS and the reflective RIS against the number, K, of RedRIS ports or reflective RIS elements. There, it is seen that the fully-connected RedRIS significantly outperforms the widely studied reflective RIS in the multi-cell setup. However, a more pronounced performance degradation is now observed (as compared to the single-cell scenario) due to reducing the number of effective RedRIS
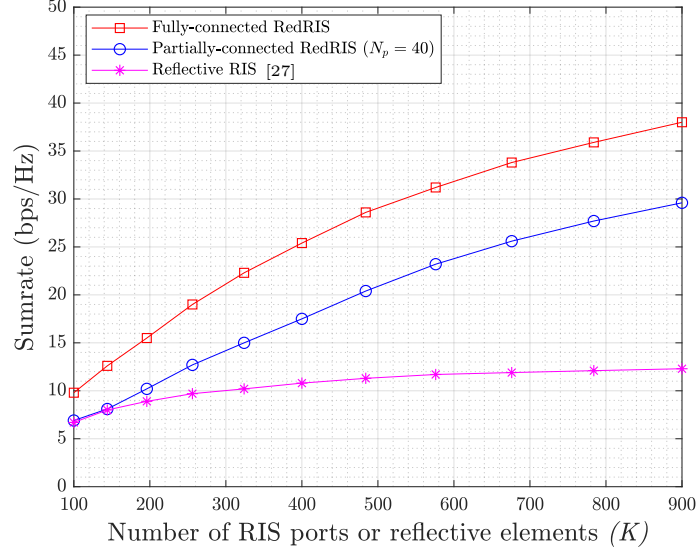
Figure 4.2: Sum-rate versus the number of RIS ports or reflection elements with $M = 8$, $BS = 8$ and $P = 30$ dBm. A LOS components are present in the BS-RIS channel only.
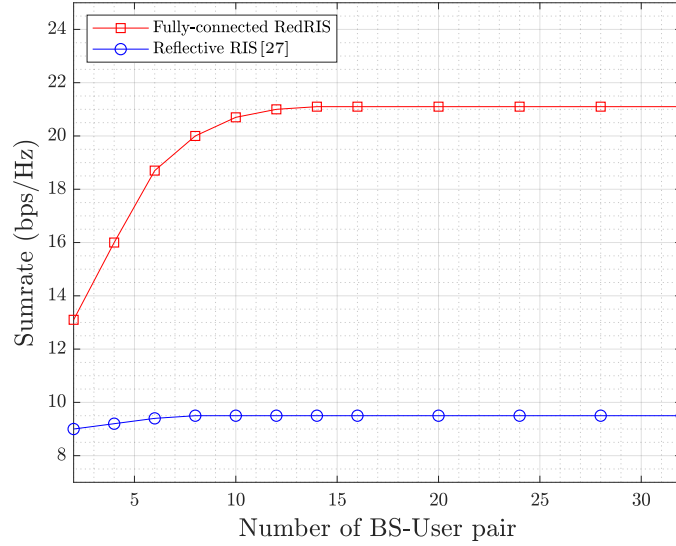

Figure 4.3: Sum-rate versus the number of BS-user pair. with $K = 256$ and $P = 30$ dBm. A LOS components are present in the BS-RIS channel only.

port connections for the sake of overhead and computational complexity savings. Yet, the achieved sum-rate even with the partially-connected RedRIS is still much higher than that of the reflective RIS. With the increase of the number of RedRIS ports and reflective RIS elements, the gap between the sum-rate curves widens. Fig. 4.3 plots the sum-rate versus the number of BS-user pair for the multi-cell setup where the sum-rate with RedRIS increases up to a certain number of BS-user pairs and then saturates. With the increase of the number of BS-user pairs, the inter-cell interference also increases which limits any further gain in the sum-rate. The flat-line in the curve corresponds to the interference-limited regime. This shows that the sum-rate with RedRIS saturates at a higher value than the reflective RIS.

4.4   Summary

In this chapter, we extended the framework introduced in Chapter 3 to a multi-cell network. We used the newly developed optimization algorithm in Chapter 3 to optimize the ports switching matrix of the RedRIS. We formulated a joint optimization problem to maximize the spectral efficiency of the users by minimizing the sum MMSE of all users' received symbols in the multi-cell scenario. We optimized the different receive scaling factors in closed-form expressions. The ports switching matrix of the RedRIS was optimized iteratively using the proposed algorithm. Finally, the simulation results revealed that the proposed RedRIS-based solution, also performs better than the conventional reflective RIS-based solution in the multi-cell network.

Chapter 5

Conclusion and Future Directions

5.1 Concluding Remarks

RIS-aided wireless communication networks have been emerged as a recent technology and have received significant attention for their capability to enhance the spectral efficiency. Moreover, RIS can be an integral part of the next generation 6G technology for their diversified applications. In this thesis, we introduced the concept of using lens-type surface as redirective RIS (RedRIS) and provided a general framework for the optimization of the switching matrix of RedRIS ports. In Chapter 3, we considered a RedRIS-assisted multi-user MIMO communication scheme in a single-cell network and formulated a joint optimization problem to maximize the spectral efficiency of each user. We developed an alternating algorithm to optimize the switching matrix of the RedRIS ports. We also developed two methods to effectively reduce the number of port connections in large-sized RedRIS without impacting the performance. In Chapter 4, we extended the framework to multi-cell network and successfully used the newly developed algorithm to optimize the RedRIS swithcing matrix along with the different receive scaling factors. We provided the simulation results for both cases and concluded

that the RedRIS-based approach outperforms the widely-studied conventional reflective RIS-based schemes in terms of achieved throughput. Also, the RedRIS outperforms the reflective RIS with reduced number of connected ports. The main advantage of the RedRIS over the reflective RIS is the achievement of better performance with less incurred control overhead that reduces the overall complexity of the RIS-assisted systems.

5.2 Future Directions

Possible extension of this work may include but not limited to the following ideas:

5.2.1 RIS-based Channel Estimation

In RIS-assisted communication system, channel state information is assumed to be known at prior. Acquisition of timely and accurate CSI is vital in RedRIS-based MIMO wireless networks. Majority of the existing research assume perfect CSI is available at the BS for the analysis. However, in practical aspect, the acquisition of accurate CSI is challenging. Related research can be performed by applying deep learning-based methods to estimate the channel information in RedRIS-based systems [10].

5.2.2 Digital Intelligent Surface

In the proposed framework, we considered the RedRIS to be a passive element without the capability of performing any digital signal processing in the incident signal. Future work can be done in designing an intelligent RedRIS that can dynamically perform necessary signal processing to further enhance the spectral efficiency and throughput of the network.

5.2.3   RedRIS in Multi-User Multi-Cell MIMO Communication

The proposed framework considers the RedRIS-aided network in multi-user single-cell and in multi-cell (each cell serving single user) cluster scenarios. Further research can be performed to extend the framework to assess the performance of RedRIS in a multi-user multi-cell MIMO communication system.

Bibliography

[1] M. A. ElMossallamy, H. Zhang, L. Song, K. G. Seddik, Z. Han, and G. Y. Li, "Reconfigurable intelligent surfaces for wireless communications: Principles, challenges, and opportunities," *IEEE Transactions on Cognitive Communications and Networking*, vol. 6, no. 3, pp. 990–1002, 2020.

[2] Q. Wu, S. Zhang, B. Zheng, C. You, and R. Zhang, "Intelligent reflecting surface-aided wireless communications: A tutorial," *IEEE Transactions on Communications*, vol. 69, no. 5, pp. 3313–3351, 2021.

[3] Z. Chen, B. Ning, C. Han, Z. Tian, and S. Li, "Intelligent reflecting surface assisted terahertz communications toward 6g," *IEEE Wireless Communications*, vol. 28, no. 6, pp. 110–117, 2021.

[4] I. F. Akyildiz, C. Han, and S. Nie, "Combating the distance problem in the millimeter wave and terahertz frequency bands," *IEEE Communications Magazine*, vol. 56, no. 6, pp. 102–108, 2018.

[5] H.-J. Song and N. Lee, "Terahertz communications: Challenges in the next decade," *IEEE Transactions on Terahertz Science and Technology*, vol. 12, no. 2, pp. 105–117, 2022.

[6] Q. Wu and R. Zhang, "Intelligent reflecting surface enhanced wireless network: Joint active and passive beamforming design," in *2018 IEEE Global Communications Conference (GLOBECOM)*, 2018, pp. 1–6.

[7] Y.-C. Liang, R. Long, Q. Zhang, J. Chen, H. V. Cheng, and H. Guo, "Large intelligent surface/antennas (lisa): Making reflective radios smart," *Journal of Communications and Information Networks*, vol. 4, no. 2, pp. 40–50, 2019.

[8] Q. Wu and R. Zhang, "Intelligent reflecting surface enhanced wireless network via joint active and passive beamforming," *IEEE Transactions on Wireless Communications*, vol. 18, no. 11, pp. 5394–5409, 2019.

[9] M. D. Renzo, M. Debbah, D.-T. Phan-Huy, A. Zappone, M.-S. Alouini, C. Yuen, V. Sciancalepore, G. C. Alexandropoulos, J. Hoydis, H. Gacanin *et al.*, "Smart radio environments empowered by reconfigurable ai meta-surfaces: An idea whose time has come," *EURASIP Journal on Wireless Communications and Networking*, vol. 2019, no. 1, pp. 1–20, 2019.

[10] Y. Liu, X. Liu, X. Mu, T. Hou, J. Xu, M. Di Renzo, and N. Al-Dhahir, "Reconfigurable intelligent surfaces: Principles and opportunities," *IEEE Communications Surveys & Tutorials*, vol. 23, no. 3, pp. 1546–1577, 2021.

[11] B. Yang, X. Cao, C. Huang, Y. L. Guan, C. Yuen, M. Di Renzo, D. Niyato, M. Debbah, and L. Hanzo, "Spectrum-learning-aided reconfigurable intelligent surfaces for "green" 6g networks," *IEEE Network*, vol. 35, no. 6, pp. 20–26, 2021.

[12] W. Yan, X. Yuan, Z.-Q. He, and X. Kuai, "Passive beamforming and information transfer design for reconfigurable intelligent surfaces aided multiuser mimo systems," *IEEE Journal on Selected Areas in Communications*, vol. 38, no. 8, pp. 1793–1808, 2020.

[13] Y. Yang, B. Zheng, S. Zhang, and R. Zhang, "Intelligent reflecting surface meets ofdm: Protocol design and rate maximization," *IEEE Transactions on Communications*, vol. 68, no. 7, pp. 4522–4535, 2020.

[14] A. Mezghani, F. Bellili, and E. Hossain, "Nonlocal reconfigurable intelligent surfaces for wireless communication: Modeling and physical layer aspects," *arXiv preprint arXiv:2210.05928*, 2022.

[15] A. Zappone, M. Di Renzo, F. Shams, X. Qian, and M. Debbah, "Overhead-aware design of reconfigurable intelligent surfaces in smart radio environments," 2020. [Online]. Available: https://arxiv.org/abs/2003.02538

[16] S. V. Hum and J. Perruisseau-Carrier, "Reconfigurable reflectarrays and array lenses for dynamic antenna beam control: A review," *IEEE Transactions on Antennas and Propagation*, vol. 62, no. 1, pp. 183–198, 2014.

[17] B. Zheng, C. You, and R. Zhang, "Double-irs assisted multi-user mimo: Cooperative passive beamforming design," *IEEE Transactions on Wireless Communications*, vol. 20, no. 7, pp. 4513–4526, 2021.

[18] J. Kim, S. Hosseinalipour, T. Kim, D. J. Love, and C. G. Brinton, "Multi-irs-assisted multi-cell uplink mimo communications under imperfect csi: A deep reinforcement learning approach," in *2021 IEEE International Conference on Communications Workshops (ICC Workshops)*, 2021, pp. 1–7.

[19] Q. Wu and R. Zhang, "Beamforming optimization for wireless network aided by intelligent reflecting surface with discrete phase shifts," *IEEE Transactions on Communications*, vol. 68, no. 3, pp. 1838–1851, 2020.

[20] M.-M. Zhao, Q. Wu, M.-J. Zhao, and R. Zhang, "Intelligent reflecting surface enhanced wireless networks: Two-timescale beamforming optimization," *IEEE Transactions on Wireless Communications*, vol. 20, no. 1, pp. 2–17, 2021.

[21] Q. Wu and R. Zhang, "Beamforming optimization for intelligent reflecting surface with discrete phase shifts," in *ICASSP 2019 - 2019 IEEE International Conference on Acoustics, Speech and Signal Processing (ICASSP)*, 2019, pp. 7830–7833.

[22] H. Yang, Z. Xiong, J. Zhao, D. Niyato, L. Xiao, and Q. Wu, "Deep reinforcement learning-based intelligent reflecting surface for secure wireless communications," *IEEE Transactions on Wireless Communications*, vol. 20, no. 1, pp. 375–388, 2021.

[23] S. Abeywickrama, R. Zhang, Q. Wu, and C. Yuen, "Intelligent reflecting surface: Practical phase shift model and beamforming optimization," *IEEE Transactions on Communications*, vol. 68, no. 9, pp. 5849–5863, 2020.

[24] P. Wang, J. Fang, X. Yuan, Z. Chen, and H. Li, "Intelligent reflecting surface-assisted millimeter wave communications: Joint active and passive precoding design," *IEEE Transactions on Vehicular Technology*, vol. 69, no. 12, pp. 14 960–14 973, 2020.

[25] C. Huang, A. Zappone, G. C. Alexandropoulos, M. Debbah, and C. Yuen, "Reconfigurable intelligent surfaces for energy efficiency in wireless communication," *IEEE Transactions on Wireless Communications*, vol. 18, no. 8, pp. 4157–4170, 2019.

[26] E. Basar, M. Di Renzo, J. De Rosny, M. Debbah, M.-S. Alouini, and R. Zhang, "Wireless communications through reconfigurable intelligent surfaces," *IEEE Access*, vol. 7, pp. 116 753–116 773, 2019.

[27] H. Ur Rehman, F. Bellili, A. Mezghani, and E. Hossain, "Joint active and passive beamforming design for irs-assisted multi-user mimo systems: A vamp-based approach," *IEEE Transactions on Communications*, vol. 69, no. 10, pp. 6734–6749, 2021.

[28] Y. Zhang and A. Alkhateeb, "Learning reflection beamforming codebooks for arbitrary ris and non-stationary channels," *arXiv preprint arXiv:2109.14909*, 2021.

[29] H. Ur Rehman, "Reconfigurable intelligent surface-assisted multi-user wireless communications systems," *MSpace University of Manitoba Thesis Repository*, 2021. [Online]. Available: http://hdl.handle.net/1993/35822

[30] C. Liaskos, S. Nie, A. Tsioliaridou, A. Pitsillides, S. Ioannidis, and I. Akyildiz, "A new wireless communication paradigm through software-controlled metasurfaces," *IEEE Communications Magazine*, vol. 56, no. 9, pp. 162–169, 2018.

[31] S. Hu, F. Rusek, and O. Edfors, "Beyond Massive MIMO: The Potential of Data Transmission With Large Intelligent Surfaces," *IEEE Transactions on Signal Processing*, vol. 66, no. 10, pp. 2746–2758, 2018.

[32] C. Pan, H. Ren, K. Wang, W. Xu, M. Elkashlan, A. Nallanathan, and L. Hanzo, "Multicell mimo communications relying on intelligent reflecting surfaces," *IEEE Transactions on Wireless Communications*, vol. 19, no. 8, pp. 5218–5233, 2020.

[33] D. P. Bertsekas, "Nonlinear programming," *Journal of the Operational Research Society*, vol. 48, no. 3, pp. 334–334, 1997.

[34] S. Rangan, P. Schniter, and A. K. Fletcher, "Vector approximate message passing," *IEEE Transactions on Information Theory*, vol. 65, no. 10, pp. 6664–6684, 2019.

[35] M. Joham, W. Utschick, and J. Nossek, "Linear transmit processing in mimo communications systems," *IEEE Transactions on Signal Processing*, vol. 53, no. 8, pp. 2700–2712, 2005.

[36] H. Jedda, A. Mezghani, A. L. Swindlehurst, and J. A. Nossek, "Precoding under instantaneous per-antenna peak power constraint," in *2017 25th European Signal Processing Conference (EUSIPCO)*, 2017, pp. 863–867.

[37] M. A. Ghouse, "2d grid architectures for the dft and the 2d dft," *Journal of VLSI signal processing systems for signal, image and video technology*, vol. 5, no. 1, pp. 57–74, 1993.

[38] R. W. Heath Jr. and A. Lozano, *Foundations of MIMO Communication*. Cambridge University Press, 2018.

[39] H. W. Kuhn, "The hungarian method for the assignment problem," *Naval research logistics quarterly*, vol. 2, no. 1-2, pp. 83–97, 1955.